International Journal of Astrobiology

cambridge.org/ija

Chemical alteration and preservation of sedimentary/organic nitrogen isotope signatures in a 2.7 Ga seafloor volcanic sequence

L. D. Anderson[1], G. E. Bebout[1,2], M. R. M. Izawa[2,3], N. J. Bridge[3] and N. R. Banerjee[3]

[1]Lehigh University, Bethlehem, PA, 18015, USA; [2]Institute for Planetary Materials, Okayama University, 827 Yamada, Misasa, Tottori 682-0193, Japan and [3]The University of Western Ontario, London, Ontario, N6A 3K7, Canada

Research Article

Cite this article: Anderson LD, Bebout GE, Izawa MRM, Bridge NJ, Banerjee NR (2019). Chemical alteration and preservation of sedimentary/organic nitrogen isotope signatures in a 2.7 Ga seafloor volcanic sequence. *International Journal of Astrobiology* **18**, 235–250. https://doi.org/10.1017/S1473550417000441

Received: 1 June 2017
Revised: 13 October 2017
Accepted: 20 October 2017
First published online: 20 November 2017

Key words:
Nitrogen isotopes; Archæan biogeochemistry; Basalt; Palagonite; Greenstone belt

Author for correspondence:
G. E. Bebout, E-mail: geb0@lehigh.edu

Abstract

Massive to lobate volcanic flows and brecciated hyaloclastite units in the Abitibi greenstone belt allow investigation of Late Archæan seafloor alteration and associated incorporation into these rocks of nitrogen (N) biogeochemical signatures. In this suite (the Blake River Group), hyaloclastite units containing putative microbial ichnofossils are particularly enriched in large-ion lithophile elements (K, Rb, Ba, Cs), B, and Li, consistent with their having experienced the greatest fluid–rock interaction during subseafloor hydrothermal alteration. Similarly, silicate-$\delta^{18}O$ and $\delta^{15}N$ values for samples from the hyaloclastites show the greatest shifts from plausible magmatic values. The chemical and isotopic patterns in these tholeiitic igneous rocks greatly resemble those in modern altered seafloor basalts, consistent with the preservation of an Archæan seafloor alteration signature. The N enrichments and shifts in $\delta^{15}N$ appear to reflect stabilization of illite and interaction with fluids carrying sedimentary/organic signatures. Enrichments of N (and the $\delta^{15}N$ of this N) in altered glass volcanic rocks on Earth's modern and ancient seafloor point to the potential utility of N for tracing past and present biogeochemical processes in similar rocks at/near the Mars surface.

Introduction

The Archæan Eon (3.8–2.5 Ga) predates the partial oxygenation of the atmosphere (~2.4–2.3 Ga; Holland 2006; Kump 2008), but multiple lines of evidence demonstrate that many different life forms arose during this period, with evidence of biologic activity possibly as early as 3.7 Ga (Rosing 1999). The earliest life forms evolved metabolisms that enabled them to survive and thrive in predominantly anoxic, reducing oceans rich in dissolved Fe^{2+} and NH_4^+, and which probably contained very low concentrations of NO_3^-, SO_4^{2-}, H_2S and non-ferrous trace metals (e.g. Beaumont & Robert 1999; Anbar & Knoll 2002). Photosynthesizing cyanobacteria may have appeared as early as ~2.8 Ga (Brocks *et al.* 1999; Falkowski & Godfrey 2008), providing localized sources of O_2 in an otherwise O-depleted environment. Beneficiaries of the small quantities of O_2 likely included the chemolithoautotrophs, which used it as an electron acceptor for their metabolisms (Godfrey & Falkowski 2009). Nitrogen (N) is essential to all known forms of life. Biological activity leads to significant fractionation of N isotopes with positive shifts in $\delta^{15}N$ up to ~10–20‰ (Fogel 2010), which may be preserved in the geological record under suitable circumstances. Nitrogen concentrations and isotopic compositions of the rocks of the Hurd Property appear to record the input of sedimentary organic N during seafloor hydrothermal alteration, implying that those signatures have been preserved for ~2.7 Gyr.

Many geochemical studies of Precambrian life have focused on kerogen and detrital mineral records preserved in low-grade metasedimentary sequences (e.g. Beaumont & Robert 1999; Jia & Kerrich 2004; Hashizume *et al.* 2006; Pinti *et al.* 2007; Garvin *et al.* 2009; Thomazo *et al.* 2010; Godfrey *et al.* 2013; Thomazo & Papineau 2013). There also is evidence for microbial activity in modern basaltic rocks (e.g. Furnes *et al.* 1996; Fisk *et al.* 1998; Furnes *et al.* 2004; Banerjee *et al.* 2006; Staudigel *et al.* 2006) and their ancient metamorphosed equivalents (e.g. Banerjee *et al.* 2007; Staudigel *et al.* 2008). Occurrences of possible Archæan microbial ichnofossils, which closely resemble modern tubular and granular structures thought to be produced by euendolithic microorganisms in modern seafloor glasses, have received considerable attention because of their possible implications for our understanding of the earliest life on Earth (e.g. Schopf 2004; Furnes *et al.* 2007), and for astrobiology (Izawa *et al.* 2010). The oldest such fossils identified with high degrees of confidence include

CAMBRIDGE UNIVERSITY PRESS

those found in volcanic glasses from the ~3.4–3.5 Ga basalt pillow rims and inter-pillow hyaloclastite units in the Hooggenoeg and Kromberg Formations of the Barberton greenstone belt in South Africa (Furnes *et al.* 2004; Banerjee *et al.* 2006; Staudigel *et al.* 2006), and in the ~3.35 Ga pillow basalts in the Euro Basalt of the Pilbara Craton, Western Australia (Banerjee *et al.* 2007). Possible ichnofossils consisting of tubular and granular aggregates of fine-grained titanite have been documented by Bridge *et al.* (2010) in a unit of brecciated volcanic rocks at the Hurd Property, a ~2701 ± 1 Ma outcrop (Ayer *et al.* 2002) in the Southern Volcanic Zone (SVZ) of the Abitibi greenstone belt (AGB). The outcrop exhibits low-temperature, greenschist-facies metamorphism thought to largely reflect hydrothermal alteration during emplacement on the Archæan seafloor without obvious overprinting by later regional-scale metamorphism (see the discussion in Bridge *et al.* 2010; also Hannington *et al.* 2003). Bridge *et al.* (2010) placed the original ichnofossil discovery into an inferred physical volcanological context. In this paper, we present new field, petrographic and geochemical observations (including major and trace element and silicate N and O isotope data) bearing on the nature of the volcanic protolith of the Hurd volcanics and their subsequent alteration during seafloor hydrothermal fluid–rock interaction. We discuss the possibility that the elevated N concentrations and shifts in $\delta^{15}N$ values in these rocks, relative to the compositions of likely protoliths, reflect additions of sedimentary/organic N during chemical/isotopic alteration that is in general similar to that observed on the modern and Mesozoic seafloor (see Li *et al.* 2007; Bebout *et al.* 2017).

Geologic setting

The AGB (Fig. 1) is one of the most extensively studied greenstone belts in the world, as both the youngest (~2.7 Ga: Ayer *et al.* 2002) and largest (~700 × 300 km; Card 1990) of the Archæan terranes (e.g. Dimroth *et al.* 1982, 1983a, b; Mueller *et al.* 1996; Mueller & Daigneault 2006). Located on the Superior Craton of Canada and stretching west–east across the Ontario–Québec border (see Fig. 1 inset), the AGB is interpreted as a volcanic arc collage that evolved over a time span of 90 Myr (Mueller *et al.* 1996). The Hurd outcrop is located within the Blake River Segment (BRS), which constitutes one of the two tectonic blocks of the fault-bounded SVZ of the AGB (Fig. 1). Formation of the volcanic arc, represented by the SVZ, occurred during the earliest stage of the greenstone belt's development, ~2730–2698 Ma, prior to the subduction of the SVZ under the older arc represented by the Northern Volcanic Zone (Mueller *et al.* 1996; Pearson & Daigneault 2009). Bridge *et al.* (2010; also see Bridge 2008) provided a comprehensive description of the geologic setting of the BRS.

The Abitibi Subprovince has a complex tectonic history, involving regional transpressional subduction, accretion, transcurrent faulting and exhumation; however, the central part of the BRS was largely protected from deformational processes and regional metamorphic overprinting. With the exception of the areas proximal to the large fault zones (the DPMFZ and CLLFZ; Fig. 1), the BRS represents a low-strain domain largely preserving original rock fabrics and textures (Dimroth *et al.* 1983a; Mueller *et al.* 1996). The Hurd Property outcrop is located in Harker Township, Ontario, Canada, north of the Town of Kirkland Lake (48.48°N, 79.77°W). It is a part of the Kinojevis assemblage, which contains tholeiitic mafic and minor felsic volcanic units (Berger & Amelin 1999) and likely formed during a period of subaqueous, basal shield volcano building (Bridge *et al.* 2010). The Hurd outcrop is located near a site with a U-Pb zircon age of 2701 ± 1 Ma (Ayer *et al.* 2002) and is likely similar in age. Given the interior position of the Hurd outcrop in the BRS and its well-preserved, recognizable volcanic textures, the chemical trends demonstrated in this study are considered to reflect the seafloor alteration processes that occurred penecontemporaneously with magmatic eruption.

The exposure has been investigated at various scales in a series of studies beginning with that of Jones (1992), who interpreted the units as spherulitic basalt and variolitic intermediate flows. Scott *et al.* (2003) argued that the units are dacitic, and Bridge (2008), Bridge *et al.* (2010) produced a high-resolution map of a ~60 × 100 m area with a 2 m grid scale (Fig. 2) and interpreted the units to be tholeiitic basalt flows. Six subvertical units of alternating lobate to massive and brecciated hyaloclastite facies are exposed at the outcrop and shown in the representative stratigraphic section in Fig. 2. The stratigraphically lowest (oldest) unit is a poorly exposed hyaloclastite of unknown thickness and from which no samples were collected in this study. The next unit up-section, also not sampled, is a 3.9 ± 1.1 m-thick, holocrystalline massive flow that grades into an overlying 3.8 ± 0.2 m-thick, brecciated hyaloclastite unit. This hyaloclastite unit is the oldest flow represented by the sample suite collected in this study and contains abundant amoeboid, holocrystalline clasts that were likely sourced from the underlying massive flow. The outcrop is volumetrically dominated by the next two younger units: a 12.0 ± 3.0 m-thick, holocrystalline massive flow containing a zone with variolitic banding at its base and grading into 0.2–2.0 m of rocks exhibiting lobate flow facies at its upper contact; and an 11.4 ± 0.6 m-thick, brecciated hyaloclastite flow unit containing lateral zonations near its top and bottom that host amoeboid-shaped, variably altered, holocrystalline clasts. The uppermost unit at this outcrop is a holocrystalline unit with an unexposed upper contact. It is slightly coarser-grained than the underlying massive flows and has an unknown thickness and origin (i.e. it could represent an intrusive sill). Unit thickness ranges were calculated using the minimum and maximum dip angles measured at the outcrop (65° and 86°; see Fig. 2) along with the minimum and maximum measured unit thicknesses (as presently exposed).

Methods

Mapping, sampling and mineralogical characterization

Detailed mapping at the Hurd Property was focused on three transects running perpendicular to the 055° baseline of the Bridge *et al.* (2010) map in the central (15 m long), eastern (25 m long) and western (40 m long) sections of the outcrop (see Fig. 2). An idealized stratigraphic section for the volcanic units was constructed by referencing the three transect maps (Fig. 2). Extensive sampling along the transects, by hammer and chisel or water-cooled, diamond-tipped rock drill, was typically at about 2 m intervals but with variation in the intervals to ensure that the dominant units and their range of lithologies were well represented. Sampling was also focused near the top of the thickest and youngest hyaloclastite unit in which Bridge *et al.* (2010) identified distinctive titanite-mineralized tubular structures suspected to be microbial trace fossils. Transmitted-light petrography was carried out using a Nikon Eclipse LV100 POL petrographic microscope equipped with a Nikon DS-Ri1 12 Mpixel camera. Petrographic analysis, combined with sample stratigraphy from mapping, enabled the selection of representative samples for geochemical analysis,

https://doi.org/10.1017/S1473550417000441 Published online by Cambridge University Press

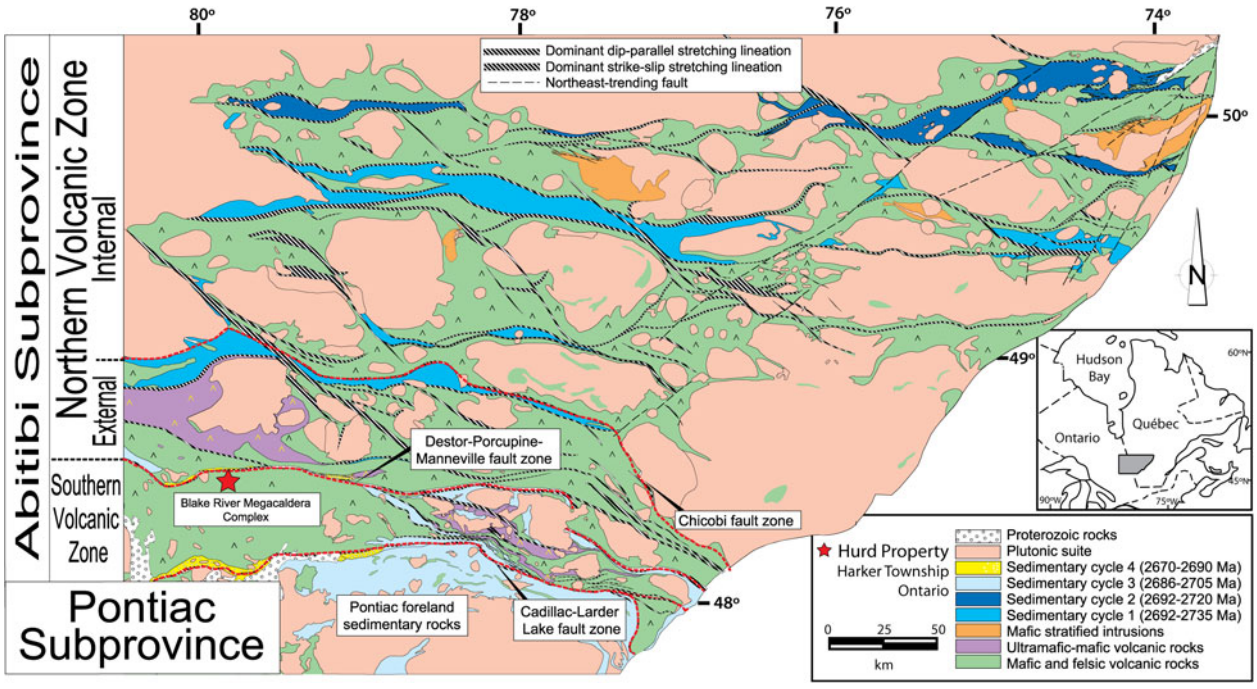

Fig. 1. General geology of the Abitibi greenstone belt, the location of the Hurd Property outcrop in the Southern Volcanic Zone is marked by the red star. Inset map shows the position of the Abitibi Subprovince on the Canadian Shield. Modified from Mueller & Daigneault (2006).

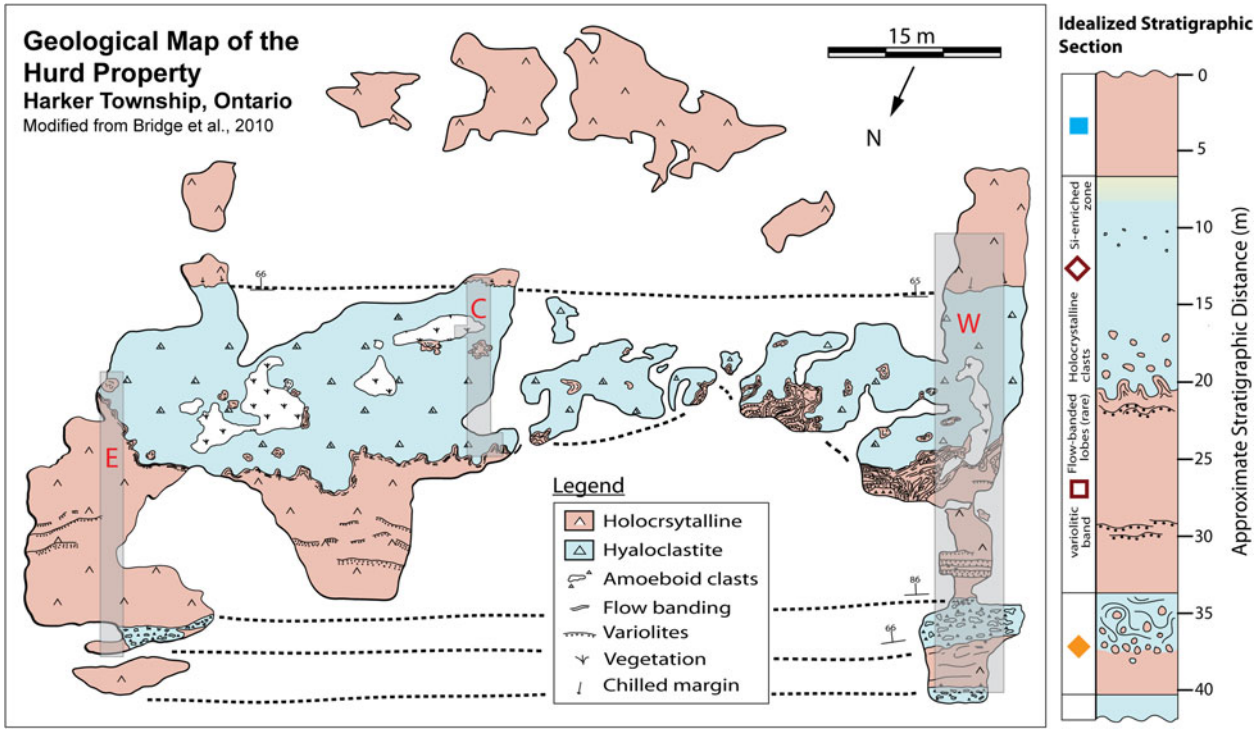

Fig. 2. Detailed map of the Hurd Property outcrop with the locations of the three transects mapped in 2008 (E, East; C, Central; W, West). Samples were collected at 2 m (or smaller) intervals within each transect, but not all were analysed for this study. The transect maps and flow thickness measurement calculations were combined into an idealized stratigraphic section (right). Diamonds and squares indicate the unit sources on samples on all following geochemical scatter plots. Map modified from Bridge *et al.* (2010).

based on sample textures and mineralogy. X-ray diffraction (XRD) analysis of bulk sample powders was performed at the University of Western Ontario (UWO), using a Rigaku Rotaflex diffractometer equipped with a rotating anode source operating at 45 kV and 160 mA, with Co Kα radiation (λ = 1.7902 Å). This work confirmed the mineralogical assemblages observed in thin section and also served to identify some trace or very fine-grained minerals indistinguishable with the petrographic microscope.

https://doi.org/10.1017/S1473550417000441 Published online by Cambridge University Press

Geochemical methods

Samples were first broken with a hammer, placed in a jaw crusher to produce rock chips, then powdered using a tungsten carbide ring mill. The major element compositions were obtained by X-ray fluorescence (XRF) spectroscopy at the UWO using a Phillips PW-1480 Wavelength Dispersive XRF unit. An extensive suite of trace elements (including REE, B, Li) was obtained from UWO and the Activation Laboratories Ltd. (Ancaster, Ontario, Canada; see methods provided by Activation Laboratories Ltd. at the following website: http://www.actlabs.com).

Analyses of whole-rock N concentrations and isotope compositions, the latter reported in standard δ notation relative to atmosphere ($\delta^{15}N_{air}$), were performed at the Lehigh University using a Finnigan MAT 252 mass spectrometer operated in carrier-gas mode and employing the methods described by Bebout *et al.* (2007; also see Li *et al.* 2007; Bebout *et al.* 2017). For these extremely low-N samples, approximately 300 mg of whole-rock sample powder were loaded into 6 mm (o.d.) quartz tubes along with 1 g of CuO_x reagent. The tubes were evacuated overnight, heated intermittently with a heat gun during evacuation and sealed under high vacuum. The sealed tubes were heated in a programmable furnace at 1050°C for 3 h, then loaded into a tube-cracker device allowing the tubes to be cracked at high vacuum to release gases into an all-metal extraction line interfaced with a Thermo Finnigan Gas Bench II carrier gas system. The N_2 was separated cryogenically from other gas phases then entrained in He carrier gas into the ion source of the mass spectrometer. Uncertainties in $\delta^{15}N$ (expressed as 1σ) are <0.15‰ for samples with >5 ppm N and increase to ~0.6‰ for samples with 1–2 ppm N (see Bebout *et al.* 2007, 2017; Li *et al.* 2007).

Silicate O isotope ratios, reported relative to ratios in Vienna Standard Mean Ocean Water ($\delta^{18}O_{VSMOW}$), were measured at the UWO, in dual-inlet mode, using a Thermo Finnigan Delta XL mass spectrometer. Approximately 9 mg of whole-rock sample powder were loaded into spring-loaded sample holders, evacuated overnight at ~150°C, and then loaded into Ni reaction vessels and evacuated for another 3 h at 200°C. The sample powders were then reacted overnight at ~580°C with ClF_3 to release the silicate-bound O (see Clayton & Mayeda 1963; Borthwick & Harmon 1982), which was then converted to CO_2 for isotopic measurement.

Results

Mineralogy and petrography

All samples experienced greenschist-facies alteration but have largely retained the primary textures of their protoliths. Thus, the prefix 'meta-' is omitted from all rock identifications for ease of reference to the dominant sample textures. Thin sections reveal a classic greenschist-facies alteration assemblage of albite, chlorite, quartz, actinolite, magnetite and calcite (Fig. 3; Appendix A). Other calcic phases typical of greenschist-facies alteration (e.g. epidote) are rare in the sample suite. The holocrystalline samples contain dominantly albite, actinolite, magnetite, chlorite, quartz and trace calcite. The dominant phases in the hyaloclastite samples are chlorite, quartz and a palagonite-like assemblage of very fine-grained clays and silica with traces of other phases (e.g. oxides, oxy-hydroxides, zeolites, titanite). These secondary phases formed by replacement of the original palagonite that represents hydration and low-temperature alteration of basaltic glass. Powder XRD analyses confirmed the presence of the dominant mineral phases: chlorite, quartz and albite, and also indicated the presence of accessory titanite, illite and trace epidote. Appendix A provides more detailed petrographic descriptions, including photomicrographs (Fig. A1) and Table A1 the latter presenting a summary of the mineralogy and textures in the holocrystalline and hyaloclastite samples.

Formerly glassy clasts within the hyaloclastite samples exhibit a wide range of shapes and textures, from cuspate, distinctly palagonite-rimmed (Fig. 3(a) and (b)); to subangular (Fig. 3(c) and (d)) and highly rounded, fractured and pervasively palagonitized (Fig. 3(e) and (f)) shards. Fine- to medium-grained chlorite, and fine- to coarse-grained magnetite and other opaque minerals (most of them probably pyrite-dominated sulfides) replaced non-palagonitized areas of the hyaloclastite glass. The chlorite is chiefly observed in the shard cores and in patches among the palagonite zones of the more heavily fractured clasts. Magnetite mostly occurs associated with chlorite. Round inclusions of quartz rimmed by a brown material, possibly a clay phase, are a less common feature within the altered clasts. A few of the hyaloclastites, specifically those with subangular to angular/cuspate clasts (Fig. 3(a) and (b)), contain tubular and granular structures of varying length and morphology filled with fine-grained titanite, which may be titanite-mineralized microbial ichnofossils (see McLoughlin *et al.* 2010). The interstices among the clasts mostly contain fine-grained quartz with some very coarse-grained (>1 mm) calcite. Chlorite is less abundant in the interstitial spaces and, where present, is commonly clustered near shard boundaries. In some samples, the clasts are very closely packed, leaving minimal interstitial space (i.e. the samples are clast-supported; Fig. 3(e) and (f)).

Major and trace element compositions

Figure 4 presents the major and some trace element data as a function of stratigraphic position. The Hurd samples contain 47–63 wt.% SiO_2, with the highest concentrations occurring in samples from the SiO_2-enriched zone at the upper contact of the thickest hyaloclastite unit (Fig. 4(l)). The TiO_2 concentrations at Hurd are 1.3–2.5 wt.%, and appear to remain relatively uniform throughout the section except in the uppermost holocrystalline unit. Concentrations of MgO and CaO in the Hurd samples (1–4 and 3–7 wt.%, respectively) are lower than concentrations in modern MORB (Fig. 4(e) and (f)). CaO and Na_2O concentrations appear to be anti-correlated (Fig. 4(e)), and K_2O is highly variable within each unit of the Hurd outcrop, especially within the hyaloclastite units (Fig. 4(h)), consistent with the influence of plagioclase. Large-ion lithophile elements (LILE) Cs, Rb, Ba, K and Sr, generally regarded as relatively fluid-mobile elements, are variably enriched in the brecciated hyaloclastite units at the Hurd Property while remaining relatively uniform in the massive holocrystalline units (Fig. 4(h), (i) and (k)). Boron and Li concentrations vary in a similar manner to the LILE, as do U and Th concentrations, with the highest concentrations of all of these elements occurring within the same horizons of the stratigraphic section (Fig. 4(j)). Hyaloclastites are enriched in fluid-mobile elements, with LILE signatures broadly consistent with subseafloor hydrothermal alteration (Fig. 5). Rare earth element (REE) patterns are generally flat, with chondrite normalized La/Yb (La/Yb_N) values close to unity (Fig. 6).

Stable isotope compositions

Eighteen samples contain 1–13 ppm N (mean ~6 ppm) and $\delta^{15}N$ values ranging from −4 to +7‰ (mean = +2‰; Fig. 4(m)). There

https://doi.org/10.1017/S1473550417000441 Published online by Cambridge University Press

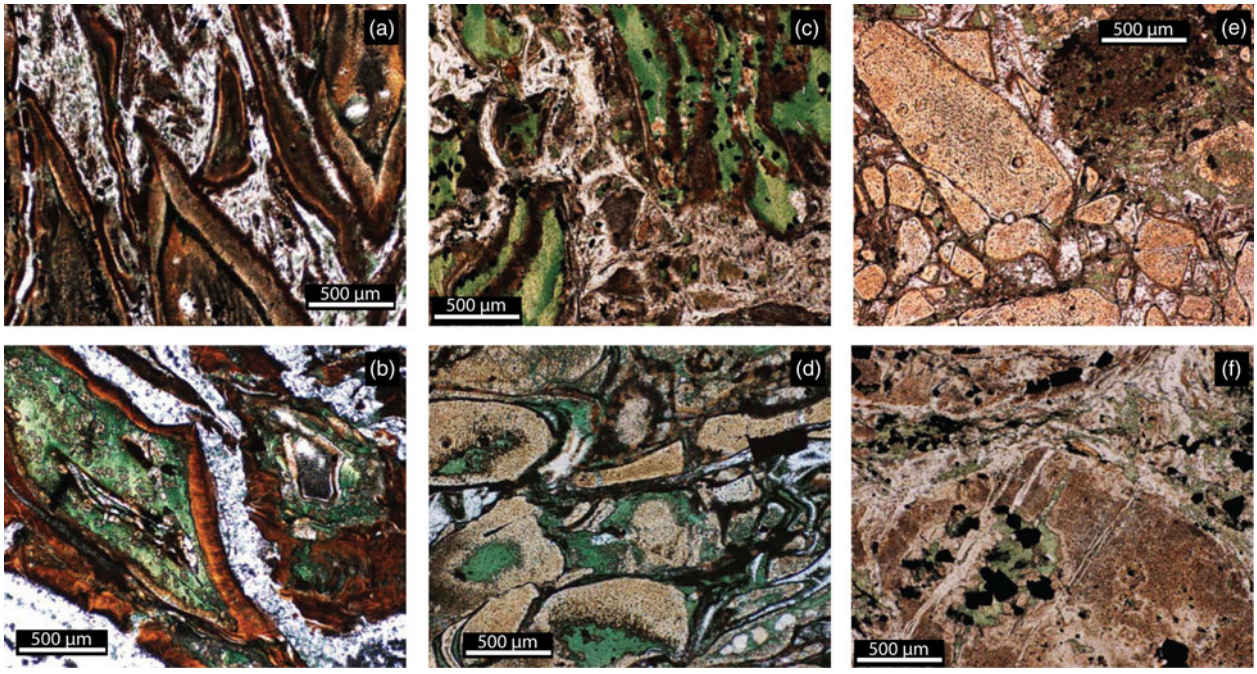

Fig. 3. Photomicrographs of the various extents of shard deformation and palagonitization exhibited in the Hurd Property hyaloclastite samples. (a) 07RN-33 and (b) 38-KH08 represent autobrecciated clasts with subangular to angular and cuspate shards rimmed with palagonite (brown). Fibrous growth texture is evident in the palagonite (b). (c) 02-KH08 and (d) 05-KH08 represent rounded and mildly fractured clasts that have non-distinct palagonite rims. (e) 03-KH08 and (f) 06-KH08 represent the most extensively fractured and palagonitized shards.

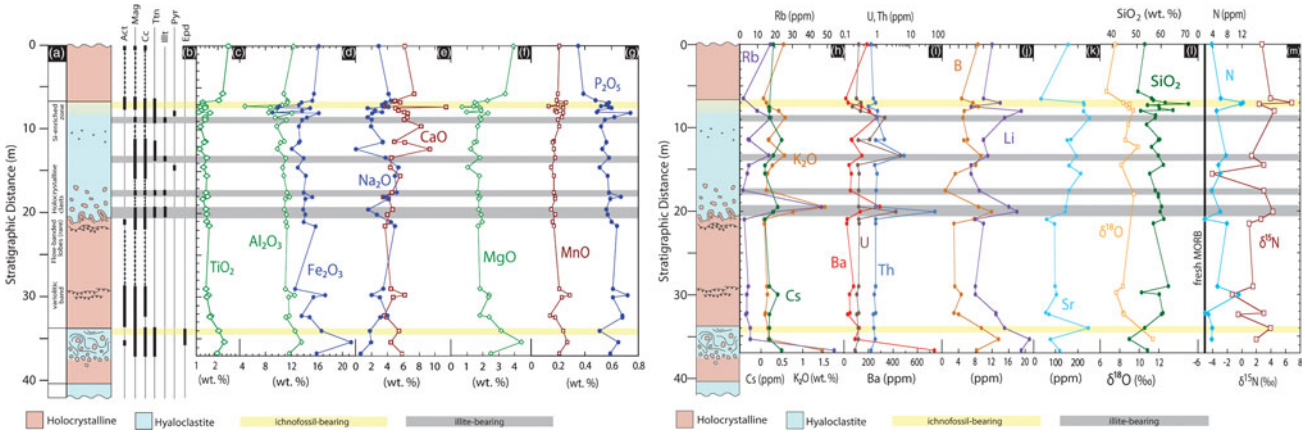

Fig. 4. Representative stratigraphic section of the volcanic units at the Hurd Property. (a) Description of volcanic facies and sample locations relative to the section. (b) Mineral occurrence diagram showing the presence of amphibole (Amp), magnetite (Mag), calcite (Cc), titanite (Ttn), illite (Illt), pyrite (Py) and epidote (Ep). Albite, chlorite and quartz have been omitted from the diagram because of their occurrence in every sample. (c–g) The major oxide element concentrations plotted as a function of their position in the section. Note that there are additional data in these plots, which are sourced from Bridge *et al.* (2010). (h–k) Large-ion lithophile and fluid-mobile element concentrations as a function of depth. (l) Oxygen isotope composition and SiO_2 concentrations. (m) Nitrogen isotope compositions and N concentrations. Horizontal shaded bars represent the ichnofossil-bearing horizons (yellow) and illite-bearing horizons (grey).

is no obvious correlation between N concentration and $\delta^{15}N$ (Fig. 7(a)). Nitrogen concentrations are weakly correlated with those of K (Fig. 7(b)), but the correlation breaks down for samples greatly enriched in K (>1000 ppm), including most of those from the thickest hyaloclastite unit.

Seventeen silicate O isotope analyses obtained in this study and nine additional analyses obtained by Bridge *et al.* (2010) show a range in $\delta^{18}O$ of +6 to +12‰ with a mean value of +8.6‰ (Fig. 4(l)). The hyaloclastites tend to exhibit $\delta^{18}O$ values most shifted from magmatic values (the latter near +6‰), suggesting that those units experienced more extensive fluid rock interactions and consistent with oxygen isotope compositions of modern altered oceanic crust. The correlated SiO_2 content and silicate $\delta^{18}O$ observed in highly silicified seafloor volcanics in the Barberton greenstone belt (Hofmann & Harris 2008) was not observed in this suite.

Discussion

A model for the eruption and alteration cycles at the Hurd outcrop, based on volcanologic, petrographic and geochemical evidence, is presented in Fig. 8 and described in the following

https://doi.org/10.1017/S1473550417000441 Published online by Cambridge University Press

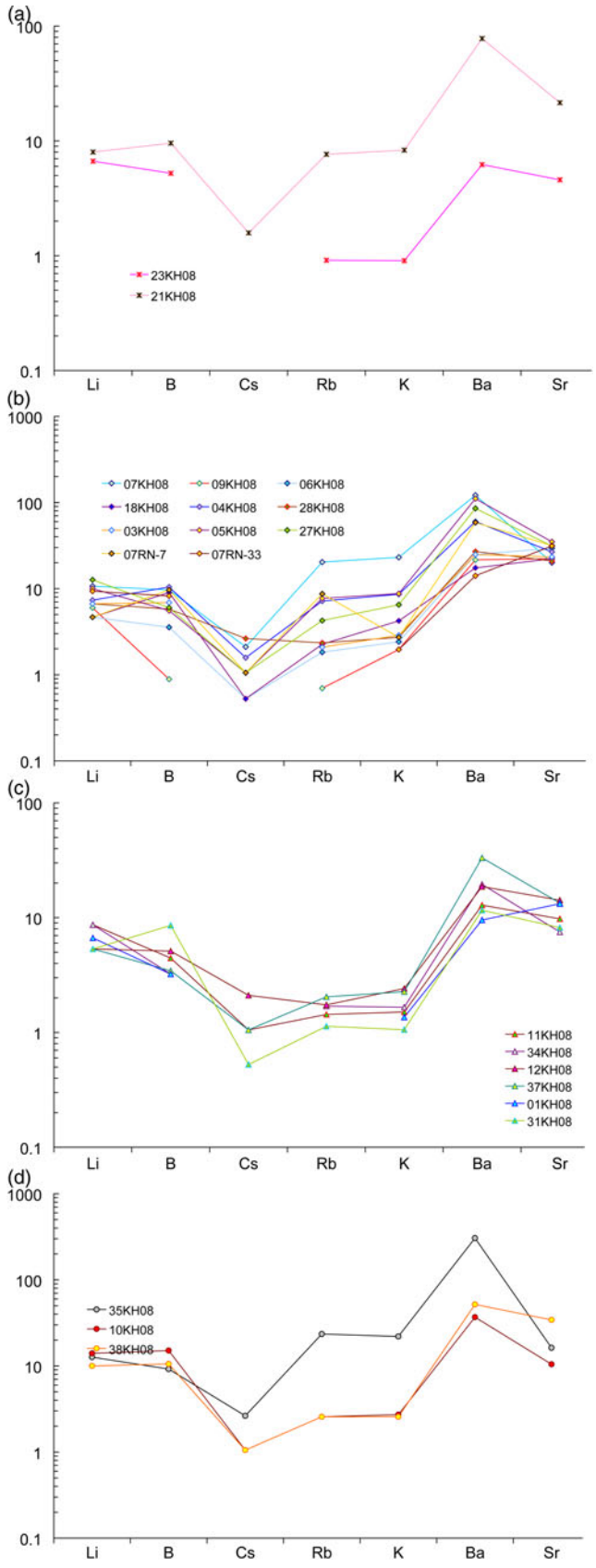

Fig. 5. Abundances of fluid-mobile elements, normalized to CI chondrites (values of McDonough and Sun 1995). (a) Uppermost stratigraphic unit, uppermost hyaloclastite unit (0–7 m); (b) thick hyaloclastite unit (7–21 m); (c) massive holocrystalline unit (21–34 m) and (d) oldest hyaloclastite (34–37 m).

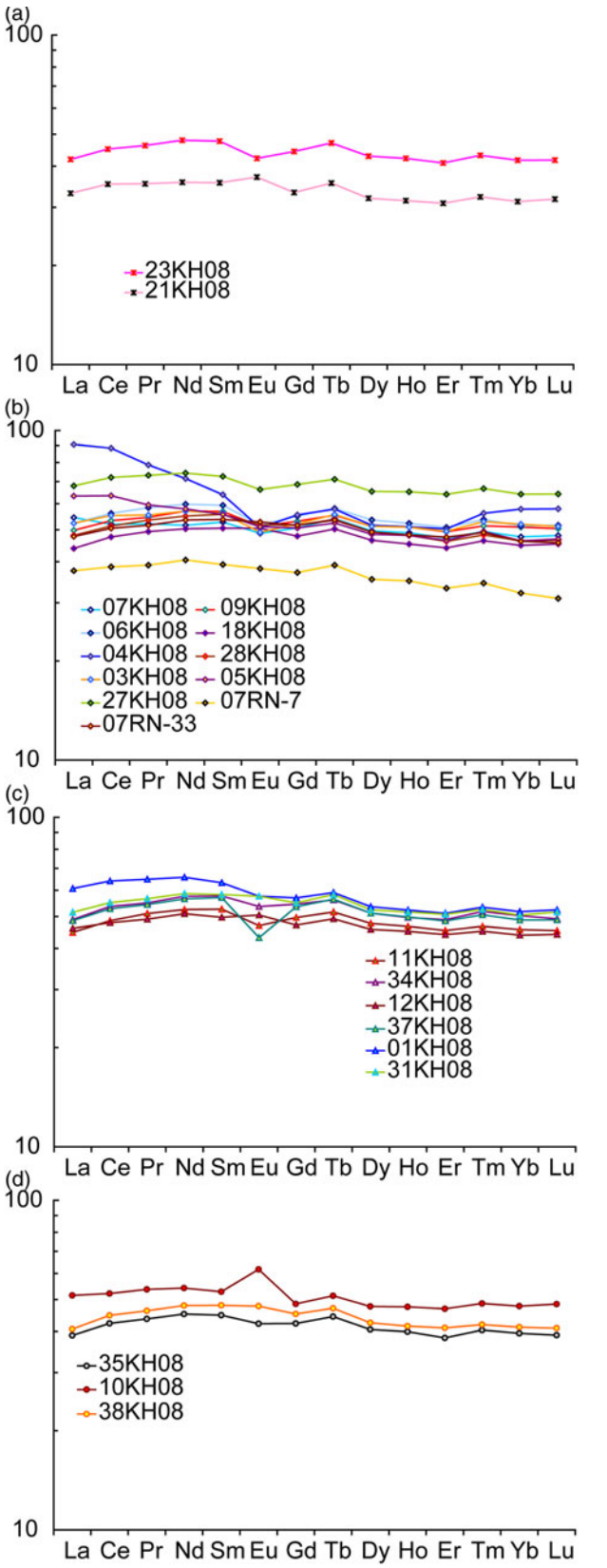

Fig. 6. Rare earth element (REE) patterns for Hurd volcanics, normalized to CI chondrites (values of McDonough and Sun 1995). (a) Uppermost stratigraphic unit, uppermost hyaloclastite unit (0–7 m); (b) thick hyaloclastite unit (7–21 m); (c) massive holocrystalline unit (21–34 m) and (d) oldest hyaloclastite (34–37 m).

https://doi.org/10.1017/S1473550417000441 Published online by Cambridge University Press

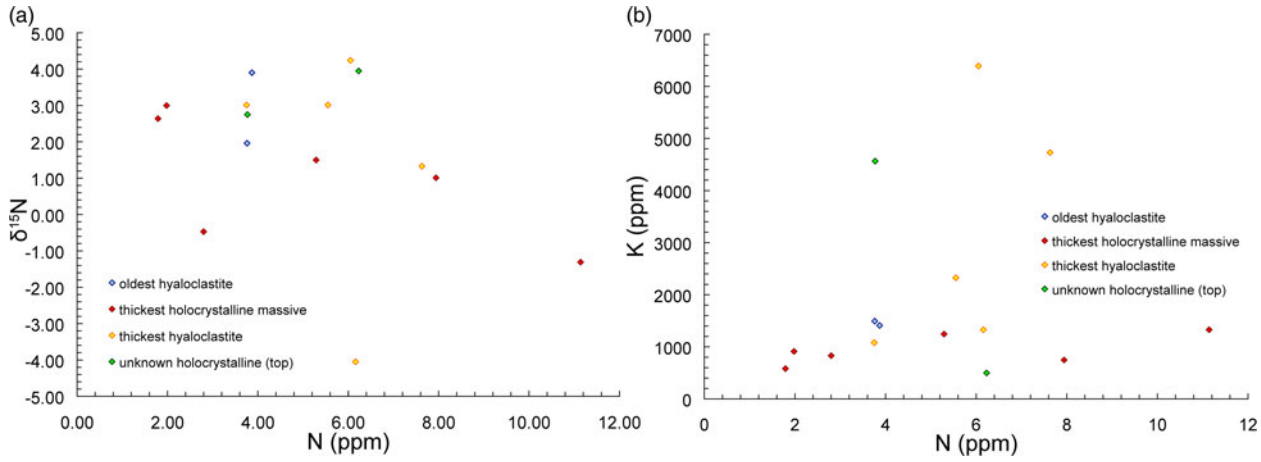

Fig. 7. Silicate-hosted N concentrations and $\delta^{15}N$ values of the Hurd Property samples. (a) N content versus isotope concentration showing no obvious correlation within the sample suite. Within each unit, however, a few trends emerge, including the Hurd unit 2b and 2c (see unit designations in Fig. 2) samples that contain ichnofossils having greater N contents than the other samples in their unit and mostly higher $\delta^{15}N$ as well. (b) Nitrogen content versus K content, showing weak correlation of N and K related to the substitution of NH_4^+ for K^+.

sections. Following eruption, each lava unit was altered by cool, infiltrating seawater that possibly introduced microbes into the glassy deposits. Later eruption events heated crustal pore waters, which produced evolved hydrothermal fluids. These hotter fluids altered the existing, cooled volcanic flows to greenschist grade, while the freshly formed, hotter lava deposited on top interacted only with cool seawater. The hydrothermal fluids likely exceeded temperatures suitable for life and silicified any remaining pore space in the older volcanic units, but the younger deposits would provide a new habitat for endolithic microbes, continuing the cycle.

Volcanic protolith

To date, the three studies considering the Hurd outcrop volcanics have proposed three different volcanic protoliths: subaqueous intermediate tholeiites (Jones 1992), subaerial dacites (Scott *et al.* 2003) and subaqueous basaltic tholeiites (Bridge *et al.* 2010). The major element oxide concentrations of the rocks were altered from initial whole-rock levels by subsequent fluid–rock interactions, so they are usually not reliable indicators of protolith composition in altered rocks. High-field strength elements, such as Ti, Zr, Nb, Ta, Y, U, Th and the REE, are regarded as being relatively immobile during fluid–rock interactions of seafloor alteration and up to mid-amphibolite facies metamorphic grades (Rollinson 1993). The trace element data obtained in this study, therefore, enable a more confident assessment of the Hurd outcrop volcanic protolith. Geochemically, the Hurd samples resemble an evolved, or intermediate, tholeiitic sequence as originally proposed by Jones (1992). The Hurd samples fall in the range of evolved magmas of andesitic to dacitic composition in the total alkali-silica diagram (Fig. 9(a); LeBas *et al.* 1986), and in the andesite range on the SiO_2-Zr/Ti diagram (Fig. 9(b); Winchester & Floyd 1977); however, the use of these discrimination diagrams for these rocks is very possibly compromised by the seafloor metasomatism experienced by the Hurd volcanics. Discrimination diagrams based on immobile elements less susceptible to the effects of hydrothermal alteration and weathering show that Hurd samples fall within the 'basaltic andesite' and 'andesite' fields (e.g. Zr/Ti versus Nb/Y ratios; see Fig. 9(c); Winchester & Floyd 1977). The tholeiitic nature of the Hurd volcanics is further demonstrated by the Th/Nb versus La/Yb discrimination diagram (Fig. 9(d); Hollocher *et al.* 2012) demonstrating MORB-like, anorogenic affinities for the Hurd volcanics. Ratios of Nb/U, U/Th and Ce/Zr remain largely uniform with increasing concentrations of the individual elements throughout the sample suite, an observation consistent with co-enrichment by progressive magmatic differentiation via fractional crystallization (Fig. 10).

Further consideration of the physical volcanology observed at the outcrop confirms an intermediate tholeiite protolith. In an idealized basaltic eruption, pillow-like flows develop between the initiating massive and terminating hyaloclastite facies as the eruption wanes (Staudigel *et al.* 1996). Commonly, when pillows are present, the hyaloclastite deposit thicknesses are minimal and may include spalled pieces of the glassy pillow rims. Volcanic pillow morphologies become far less common in more siliceous eruptions involving higher viscosity magmas and are commonly replaced with more explosive, pyroclastic eruptions and glassy deposits (Condie 1981). The two flow facies at the Hurd outcrop, a massive to lobate, holocrystalline flow and a hydroclastic, or brecciated, hyaloclastite deposit, share gradational boundaries with hyaloclastite units commonly hosting clasts from the underlying massive basalts. This indicates that the two complete volcanic cycles exposed at the Hurd outcrop never developed flows with pillow morphologies. This conclusion is also supported by the evidence for minimal deformation at the outcrop scale, which precludes the possibility that any pillowed flows that may have formed were later displaced from the stratigraphic section.

Although pillowed flows are completely absent at the Hurd outcrop, nearby outcrops of similarly aged mafic units host thick units of variolitic basalt pillows (Jones 1992). This observation indicates that coeval Archæan subaqueous basaltic eruptions were constructed in a similar manner to that of modern seafloor volcanic sections. The absence of pillowed flows at the Hurd outcrop, but presence in nearby sections, can be explained by differing magma compositions at the outcrops. Archæan andesites commonly occur primarily as tuffs, breccias and agglomerate flows where the ratio of explosive to effusive flows increases with increasing stratigraphic height and decreasing distance to eruptive centres (Condie 1981). Eruption-fed turbidity currents, where water is a continuous intergranular phase of the particulate flow, dominate these occurrences, and turbulence is a particle

https://doi.org/10.1017/S1473550417000441 Published online by Cambridge University Press

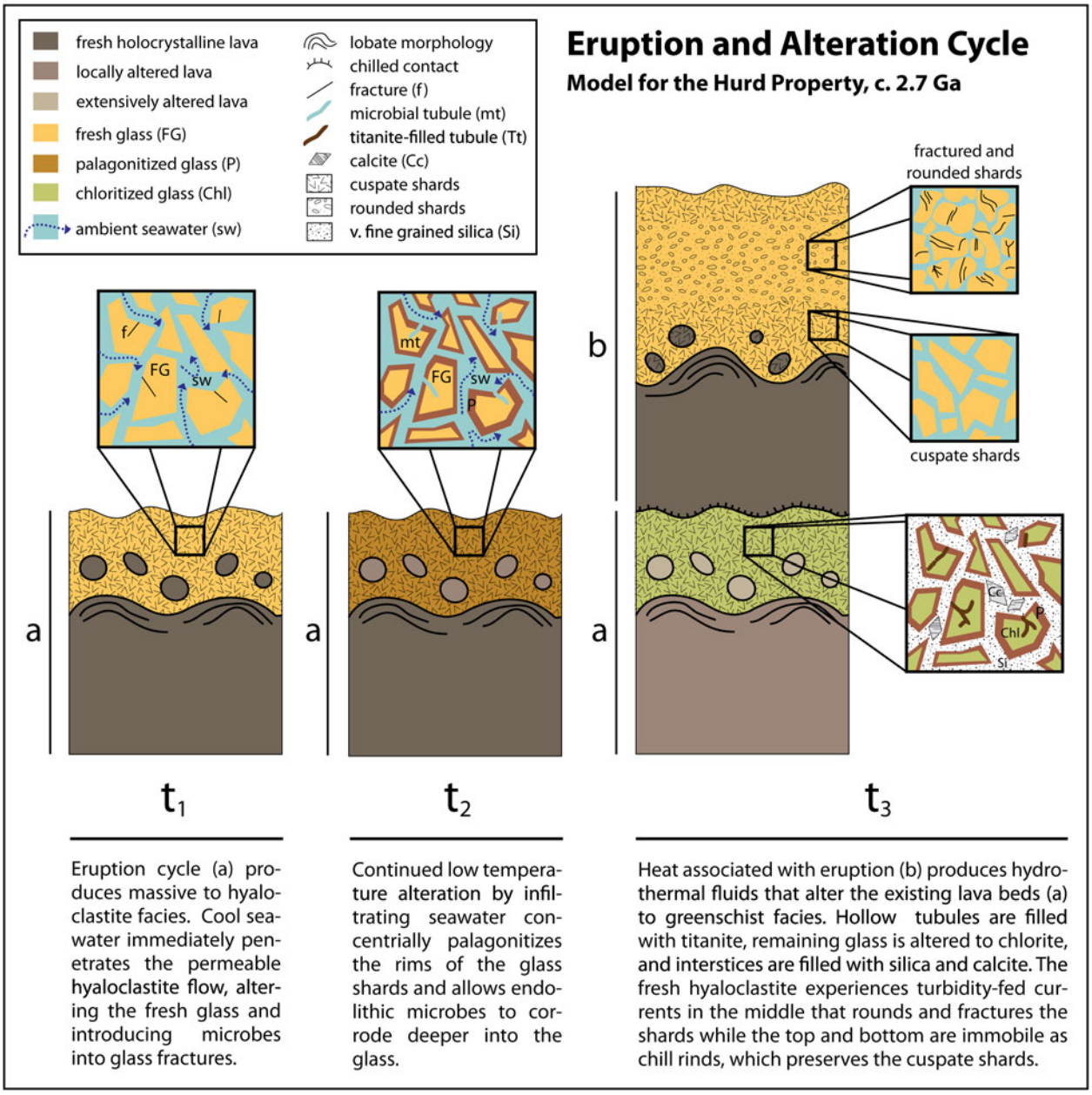

Fig. 8. Conceptual model of the eruption, alteration and microbial colonization cycles at the Hurd outcrop with a summary of events during each point in time, t_1, t_2 and t_3; (a) and (b) indicate the specific eruption cycle units. Note that flow thicknesses and effects of subsidence are not indicated because the diagram is not spatially scaled.

support mechanism (White 2004). In these turbidity currents, vertical (or lateral) segregation of the flow unit occurs, and is possibly due to, some parts of the current dominated by intergranular collisions causing extensive shard fracturing and rounding of edges. Lateral zonation is clearly evident in the thickest hyaloclastite flow at the Hurd outcrop where the middle portion is dominated by rounded and fractured glass-rich clasts, and appears to be clast-supported. This is in contrast to the upper and lower zones of the same unit where pristine cuspate clasts are preserved within a matrix of fluid-precipitated silica. The middle part of the thickest hyaloclastite deposit thus resembles the eruption-fed turbidity currents characteristic of modern subaqueous siliceous magma flows and would have flowed between two chilled rinds of autobrecciated glass that cooled immediately upon contact with old, cold seafloor below and cool seawater above.

Based on the considerations above, the volcanic protolith of the Hurd outcrop rocks was likely an intermediate tholeiitic composition of anorogenic origin, similar to an icelandite. This does not necessarily imply volcanic arc, crustal mixing or subduction-related processes. Trace element systematics of the Hurd outcrop display a tholeiitic affinity and are most consistent with a within-plate setting. An anorogenic origin for the intermediate tholeiites is also supported by the age estimate of the Hurd outcrop. The volcanic flows were erupted at ~2701 Ma (Ayer *et al.* 2002) during the subaqueous development of the shield volcano that became the SVZ (Mueller *et al.* 1996). This predates, by ~5 Ma, the earliest age of subduction between the Southern and Northern Volcanic Zones;

https://doi.org/10.1017/S1473550417000441 Published online by Cambridge University Press

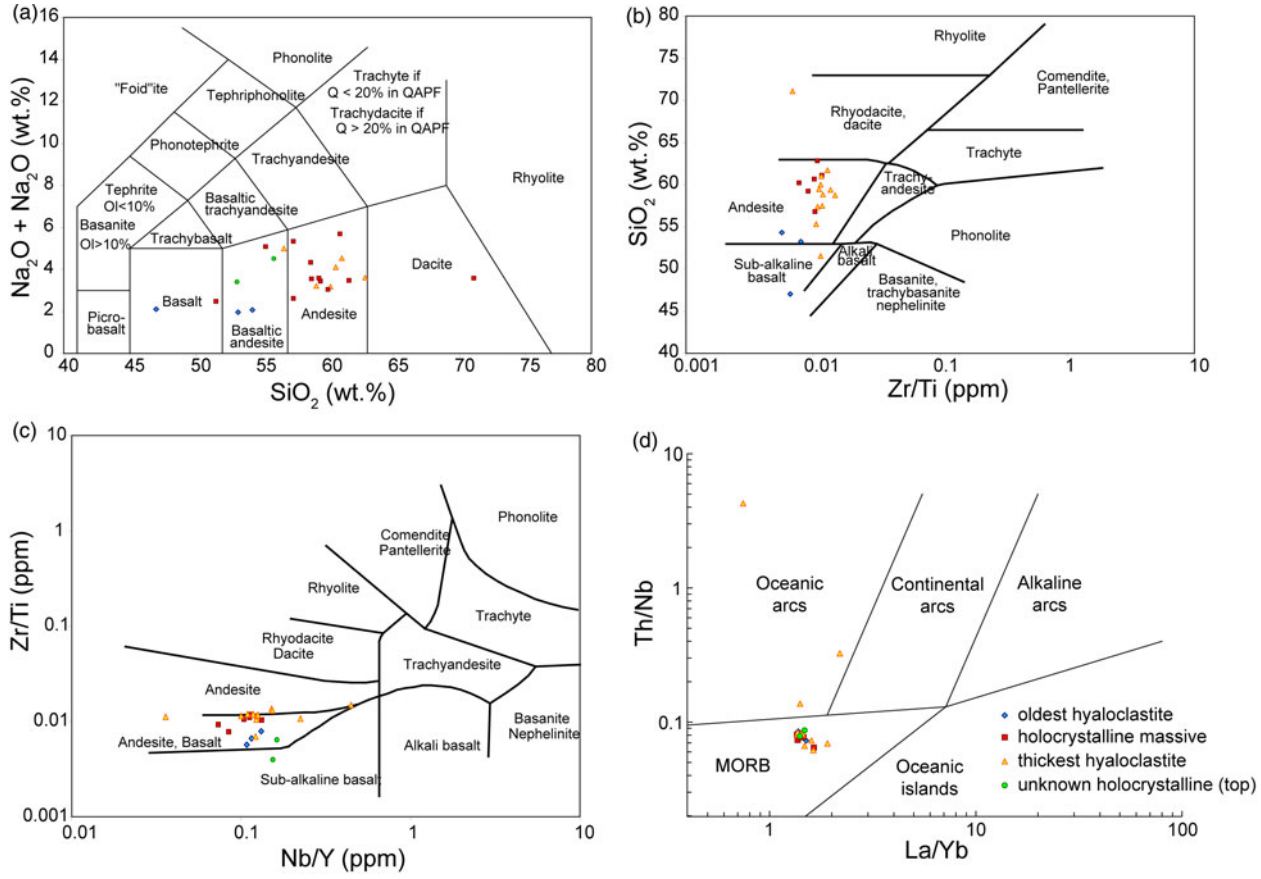

Fig. 9. Geochemical discrimination diagrams with data for the Hurd Property samples. (a) Total alkali versus silica (TAS) diagram showing the broadly tholeiitic affinity of the Hurd Property rocks. (b) Alternative discrimination diagram using Zr/Ti instead of total alkalis (which are presumably more strongly affected by post-magmatic processes), showing the same tholeiitic affinity. Volcanic classification diagrams employing high-field strength elements. (c) Zr/TiO_2 ratio versus Nb/Y ratio demonstrating the intermediate basaltic andesite to andesite nature of the Hurd Property samples. (d) TiO_2 versus Zr concentrations demonstrating the intermediate nature of the Hurd Property samples whose Ti and Zr contents resemble within-plate lavas more than they resemble volcanic arc lavas (indicating a lack of crustal contamination).

thus, crustal mixing likely was not involved in the formation of the Hurd outcrop magmas. Furthermore, fractional crystallization has been proposed for some rare andesitic to rhyolitic rocks in well-developed mafic assemblages on the Ontario side of the BRS (Jackson *et al.* 1994). The evolved units can be derived by extensive fractionation of mafic tholeiitic parent magma, which are classified as THOLKOM-type (tholeiitic–komatiitic-type) assemblages (Jackson *et al.* 1994). The Hurd Property outcrop is part of the Kinojevis assemblage, which is classified as a THOLKOM and is therefore a potential candidate for having experienced extensive fractional crystallization. It is possible that the higher heat flux from the Archæan mantle (Davies 1980) supported a shallow, more differentiated magma body in the precaldera, shield volcano-building setting.

Conceptual model of alteration

Petrographic results suggest that the Hurd outcrop samples were affected by at least two types of alteration: low-temperature seafloor alteration involving primarily seawater that resulted in glass dissolution, indicated by the palagonite phase in glass clasts (<150°C); and higher temperature hydrothermal alteration involving evolved fluids, indicated by the chlorite-replaced glass and greenschist-grade secondary mineral assemblages of the holocrystalline samples (~250–350°C). The following sections describe the inferred sequence of these paragenetic events.

Low-temperature seafloor alteration

Fluid–rock interactions at the seafloor interface constitute a large portion of global element cycling, with low-temperature basalt alteration and glass dissolution allowing the exchange of many elements between seawater and oceanic crust. Due to its amorphous and unstable structure, volcanic glass is particularly susceptible to alteration by seawater. Palagonite is the most common alteration product of glass and is described as an intermediate gel-like, heterogeneous material (Stroncik & Schmincke 2001). The gel-like palagonite is also thermodynamically unstable and is later replaced by clays and zeolites (Stroncik & Schmincke 2001). The step producing gel-like palagonite involves congruent dissolution and manifests itself in modern samples as a smooth and distinct boundary between fresh glass and the alteration material, with the alteration product progressing concentrically inwards to the shard centre (Stroncik & Schmincke 2001). This characteristic texture is observed in the cuspate glass shards of the Hurd hyaloclastites (Fig. 3(a) and (b)) where there are distinct regions of altered glass (brown palagonite rims) and preserved fresh glass now altered to chlorite. The palagonite phase in these samples is relatively free of inclusions and in some areas

https://doi.org/10.1017/S1473550417000441 Published online by Cambridge University Press

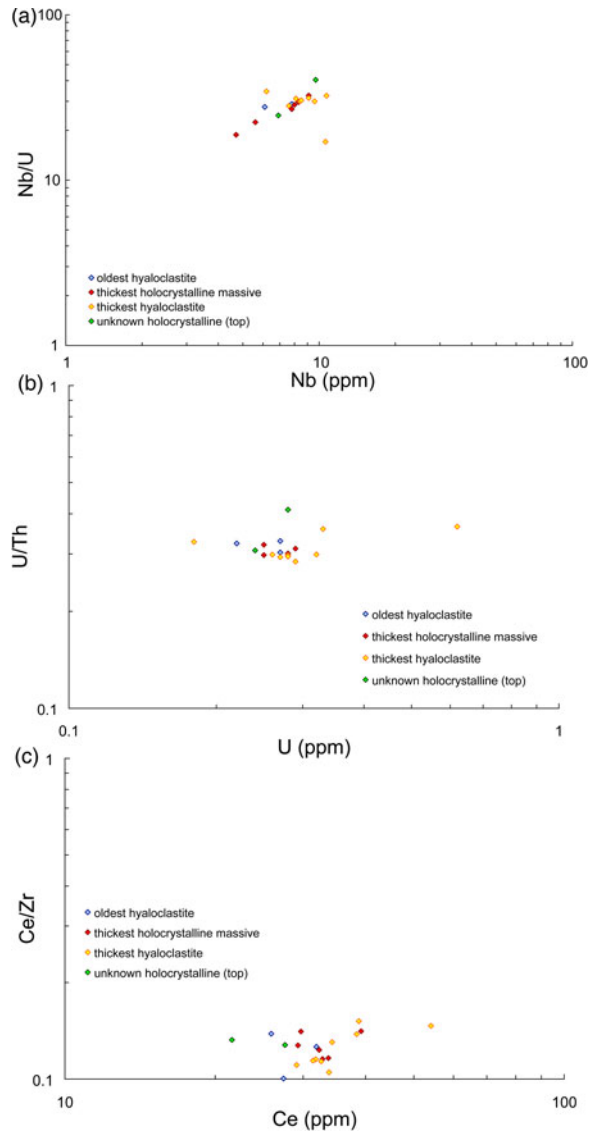

Fig. 10. Ratios of elements with similar compatibility versus concentration show uniform ratios with enrichment, consistent with by progressive magmatic differentiation via fractional crystallization. (a) Nb versus Nb/U; (b) U versus U/Th and (c) Ce versus Ce/Zr.

exhibits fibrous textures perpendicular to the glass alteration front, a common texture in crystallized palagonite (i.e. a mix of clay compositions; Stroncik & Schmincke 2001, 2002). Stroncik & Schmincke (2002) note that (gel-like) palagonite generally has a sponge-like texture with large amounts of heterogeneously distributed pores, and may contain spherical structures, which Zhou *et al.* (1992) had interpreted to be microcrystalline precursors of smectite. Textures resembling this description are found in the more rounded and fractured shards that are pervasively palagonitized (Fig. 3(c)–(f)). The rate of glass dissolution in these samples was undoubtedly catalysed by the high fracture density and increased surface area. Gel-palagonite formed quickly and non-uniformly (i.e. not in concentric layers) due to increased access of fluids into the rounded glass shards resulting in patchy or sponge-like textures that are heavily included by secondary mineral phases, including fine-grained quartz, chlorite, calcite and opaque minerals. These secondary mineral phases might have formed coevally with the silicification of the gel-like palagonite into its current crystalline phase.

Smectite is the dominant phase in modern crystallized palagonite but additional phases that commonly replace gel-like palagonite include other clay minerals, carbonates, zeolites, and Fe-, Ti- and Al-oxyhydroxides (Staudigel *et al.* 1996; Kruber *et al.* 2008). No smectite was detected in any of the hyaloclastite samples containing a palagonite phase, either optically or by XRD. Similarly, very few clay minerals, other than illite (Fig. 3(b)), and no oxyhydroxides or zeolites, were detected in parts of hyaloclastite samples thought to represent the initial palagonite. It is likely that the initial palagonite assemblage has been replaced by other phases, including illite (observed in some XRD patterns), during low-grade metamorphism. Thin section observations of former palagonite are consistent with the presence of fine-grained illite, stained with Fe-oxyhydroxides. The presence of illite is significant, as it is the only identified alteration phase that commonly incorporates elevated concentrations of K and other LILE and it is a likely mineral host for N structurally bound as NH_4^+.

Many factors influence the direction of element exchange during the formation of palagonite (Stroncik & Schmincke 2001). Studies addressing the elemental exchange between fresh and palagonitized glass pairs produce wildly differing results. Kruber *et al.* (2008) concluded that there is a near-complete loss of alkalis (Li, Na, K, Rb and Cs) from the crust during gel-palagonite formation, whereas Staudigel *et al.* (1996) suggested that there is an uptake of LILE, K, Rb and Cs during glass hydration. Furthermore, another exchange of elements and H_2O contents occur between rock and ambient fluids when the gel-palagonite crystallizes (Stroncik & Schmincke 2001). Despite the difficulty in predicting element behaviour during palagonitization, a few trends in the high-resolution element variations within the brecciated hyaloclastite and massive flow units (Fig. 4) could reflect palagonitization at the Hurd Property. The concentrations of Sr, B and Li are generally higher and more variable in the hyaloclastite units (Fig. 4(j) and (k)), likely due to exchange with seawater. This trend has been observed in modern volcanic sections by Chan *et al.* (2002), who reported Li enrichments in breccias relative to nearby massive flows in the upper volcanic section of ODP Hole 504B. Similarly, LILE enrichments in certain hyaloclastite samples could be partially due to early, low-temperature alteration, but the enrichments are not consistent throughout the entire suite of palagonite-bearing hyaloclastite samples. We thus conclude that early, low-temperature, seafloor alteration processes, which hydrated and palagonitized glass surfaces exposed to infiltrating seawater, were chemically overprinted by later hydrothermal alteration and are best inferred from the petrographic textures and mineral assemblages observed in the samples.

Hydrothermal alteration

The mineralogy of the Hurd Property samples indicates that alteration reached greenschist-grade conditions (low pressure and $250°C \leq T \leq 350°C$) at peak metamorphism. The silicate $\delta^{18}O$ data support interaction with lower temperature hydrothermal fluids, at high fluid–rock ratios, with values increased from those of fresh mantle-derived basalt (+5.7‰; Muehlenbachs & Clayton 1972; Muehlenbachs 1986). At temperatures below 200–250°C, whole rock $\delta^{18}O$ values increase in the crust because ^{18}O forms stronger bonds in the newly created secondary minerals (Bowers 1989). Gregory & Taylor (1981) quote a typical range for pillow lavas from multiple ophiolites of +10 to +14‰, representing shallow, low-temperature circulation systems. The

https://doi.org/10.1017/S1473550417000441 Published online by Cambridge University Press

Hurd sample values fall slightly below that range (+6 to +12‰; Fig. 4(l)). The $\delta^{18}O$ values are higher in the hyaloclastite samples than in the underlying holocrystalline samples from the thickest volcanic cycle, likely representing more extensive circulation and higher water/rock ratios in the hyaloclastite unit. More extensive circulation provided greater fluid volumes and a larger window of opportunity for the hyaloclastite samples to approach equilibrium than that experienced by the massive flow. The slight disparity in estimated temperatures between the mineral assemblage (estimated at 250–350°C) and O isotope compositions (<250°) likely indicates that the silicate $\delta^{18}O$ values reflect the time-integrated effect of fluid–rock interaction, including slight retrograde alteration from the maximum metamorphic grade attained, which is recorded by the secondary mineral assemblage.

Flank, or passive, hydrothermal circulation processes driven by heat conducted into the modern crust operate at temperatures of 0–150°C but account for about 85% of the total oceanic heat flux (Alt 2003; and references therein). They generally involve disseminated discharge of hydrothermal fluids through areas of the seafloor that are made permeable primarily by fracture networks or brecciated lithologies (Lowell *et al.* 1995). The hydrothermal convection cells in these passive alteration regimes are usually no more than 100–200 m deep and develop as closed circulation systems with limited or no exchange with seawater (Alt *et al.* 1996; Gutzmer *et al.* 2003). Based on the temperatures and constraints on fluid–rock ratios indicated by mineral assemblage and O isotope compositions, the hydrothermal alteration at the Hurd outcrop was likely caused by low to moderate temperature ($T <$ 350°C), shallow-circulating fluids in a flank-like setting that allowed interaction with large volumes of fluid. The fluids were heated by proximity to active magma chambers prior to or penecontemporaneously with eruptions.

The Hurd Property samples all display moderate to extensive albitization and chloritization. Two samples, 01-KH08 and 31-KH08, were selected to be the most representative of the primary magma composition. This selection was based on well-preserved primary igneous textures, low modal percentages of chlorite and major element contents consistent with average suite values. Compared to these two samples, the enrichment of MgO in more altered samples appears minor. The CaO contents are enriched in many of the samples, reflecting the presence of calcic secondary minerals including actinolite, titanite, epidote and calcite. These trends are consistent with other observations of syn-volcanic hydrothermal and low-temperature seawater interaction with mafic and felsic rocks of the eastern BRS, where spilitization (albite and chlorite replacement) is common (Hannington *et al.* 2003). Calcium enrichment associated with the formation of calcic minerals (prehnite, pumpellyite, epidote, actinolite, titanite and calcite) is especially common in the mafic rocks (Hannington *et al.* 2003). Most of the Hurd Property samples also show significant enrichment in K, Rb and Ba (Fig. 5). Trends in LILE, B, Li, U and Th concentrations (Fig. 4(h)–(k)) serve as markers of zones of the hyaloclastite units that had the highest permeability and thus were accessible to fluids for the longest periods of time (allowing the most extensive fluid–rock interaction and associated element enrichment). This conclusion is supported by the presence of illite in samples from these zones (grey-shaded bars in Fig. 4), as illite is a likely host for many of these elements (e.g. Li substitutes for Mg in octahedral sites in clays such as smectite and is also concentrated in chlorite; Chan *et al.* 2002).

A possible subsurface microbial habitat

The location of the newly identified ichnofossil-containing sample in a structurally lower (older) brecciated unit (Anderson 2010) suggests that conditions suitable for microbial seafloor inhabitation were satisfied more than once at the Hurd locality. All three of the samples containing these microbial structures exhibit cuspate shards and well-silicified interstices (see Bridge 2008). None of the hyaloclastite samples with rounded, fractured and variably palagonitized shards appear to contain ichnofossils. This may be due to a preservation bias by which the tubular structures in the cuspate, minimally palagonitized shards were the only textures unaffected long enough during seafloor alteration to be infilled with titanite during later hydrothermal alteration. Alternatively, the pattern arising from ichnofossil occurrences, only appearing at the top of hyaloclastite flow units in the proposed 'chill rind' (flow crust) zone that experienced little internal clast movement or deformation, suggests that this may have been the most favourable horizon for microbial colonization.

The cycle proposed to explain the two temporal occurrences of ichnofossils in only one breccia texture (i.e. cuspate shards; Fig. 3 (a) and (b)) begins with the eruption of a massive flow that wanes to lobate and then brecciated facies, producing a large volume of fresh volcanic glass. Glass shards in the middle of thicker hyaloclastite units likely experienced eruption-fed, density-current-like flow or compaction, which caused them to become rounded and highly fractured (Fig. 3(e) and (f)) and increased the glass surface area. These mid-section glasses were quickly and extensively altered to palagonite by circulation of cool seawater through the permeable volcanic units. In contrast, glass clasts that formed as chill-rind quench textures (i.e. autobrecciated upon contact with a cool surface like that of an underlying massive flow or the lava–seawater interface; Fig. 3(a) and (b)) retained their angularity and glassy structure, allowing the horizon to maintain well-defined, porous interstitial spaces. The minimally fractured, cuspate clasts experienced lower rates of palagonitization and alteration due to smaller surface area to volume ratios. Once the lava cooled to temperatures suitable for life, endolithic microorganisms introduced by cool circulating seawater could access and exploit the preserved glass (i.e. non-palagonitized shard interiors). Life persisted in the cuspate glasses, which were simultaneously palagonitized in the characteristic inward progressing concentric rims, as long as either actively or passively burrowing microbes stayed ahead of the reaction front marking the boundary between glass and palagonite. The microbes could have gained energy by releasing electron donors from the glass to exploit in energetic redox reactions until ambient and fluid temperatures rose above suitable levels for the organisms. Evidence of microbial bioalteration in the modern deep oceanic crust approaches maximum texture densities at ambient temperatures of ~80°C (Staudigel *et al.* 2008), and an upper limit of 121°C has been measured for the viability of thermophilic *Archaea* (Kashefi & Lovley 2003). The hydrothermal systems at the Hurd locality introduced fluids of $T < 350$°C that altered the existing volcanic rocks to greenschist-facies metamorphic assemblages. At this point, any remaining glass was altered to chlorite and the tubules were filled with titanite. The eruption(s) that heated the hydrothermal fluids also deposited a fresh layer of glass on the seafloor for continued microbial colonization of the seafloor.

By 2.7 Ga, life may have been colonizing seafloor glasses for 0.8 Gy or longer and continental crust growth was proceeding at possibly some of the greatest rates experienced to that point (Arndt 2004). Considering the abundance of Archæan volcano-

https://doi.org/10.1017/S1473550417000441 Published online by Cambridge University Press

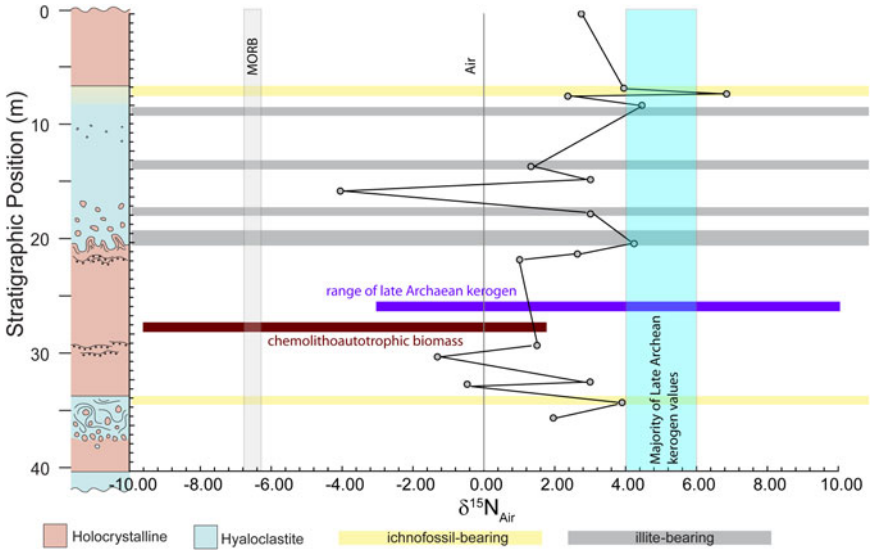

Fig. 11. Nitrogen isotope composition plotted versus stratigraphic depth for the Hurd section. Shaded fields indicate the range of most Archean kerogen, modern air and modern MORB. Horizontal bars represent estimates of the range of $\delta^{15}N$ values for two possible N input sources (chemolithoautotrophic biomass and Late Archean biomass) that could have influenced the $\delta^{15}N$ of the NH_4^+ preserved in the volcanic rocks. The Hurd samples, even those containing microbial ichnofossils, appear to largely reflect the sedimentary kerogen values, indicating that fluids likely introduced NH_4^+ derived from overlying organic-rich sedimentary units.

sedimentary sequences affected by low-temperature hydrothermal activity, of which the AGB is one, and the apparent suitability of such a habitat for modern microorganisms, it seems very likely that microbes would have exploited these ancient habitats (Hofmann & Harris 2008). Large, well-preserved greenstone belts like the AGB should provide a high potential for finding traces of life within their volcanic sequences.

Nitrogen remobilization from overlying sediments

Isotopic records of Archæan and Proterozoic rocks reflect various steps in the perturbation of the geochemical cycles into their modern biogeochemical states (e.g. Thomazo *et al.* 2010). Nitrogen leaves a significant and increasingly considered (in addition to C and S) light isotope record of evolving biogeochemical and environmental redox conditions (see Thomazo & Papineau 2013; Zerkle & Mikhail 2017). Large positive fractionations, up to 10–20‰, in $\delta^{15}N$ are known to occur via the process of denitrification, which converts NO_3^- to N_2. The process favours the lighter ^{14}N for conversion into the gas phase and leaves the remaining NO_3^-, which can be converted back into bioavailable NH_4^+, enriched in ^{15}N (Boyd 2001; Fogel 2010). The sedimentary kerogen N record is thought to preserve the isotopic values of marine organic matter in the form of NH_4^+, which represent the ^{15}N-enrichment of residual dissolved nitrate (Beaumont & Robert 1999). Values ranging from −6 to +12‰ are reported for Archæan and Proterozoic kerogens in the sedimentary record (Fig. 11). Values between +4 and +6‰ are most common, indicating the changing redox conditions of the oceans and presence of nitrifying and denitrifying microbes by the Late Archæan (Beaumont & Robert 1999).

In addition to their significance as the primary host of the fluid-derived K, potassic secondary minerals can host N in the form of NH_4^+, which has the same charge and similar ionic radius (~148 versus ~133 pm in 12-fold coordination; Shannon 1976; Holden & Dickinson 1975) to K^+. Very little silicate N was detected in the Hurd samples (~3–12 ppm); however, altered basaltic rocks and glasses on the modern and Mesozoic seafloor overlap with this range in concentration (Bebout *et al.* 2017). The low N content could reflect limited delivery of N to the rocks by fluids, poor preservation of the N as NH_4^+ and/or a low abundance of K-rich minerals in the primary and secondary mineral assemblages. There is a tenuous positive correlation between K and N concentrations (best illustrated by the thickest massive hyaloclastite unit; Fig. 7(b)), consistent with the substitution of NH_4^+ for K^+. The Pearson product-moment correlation coefficient (commonly denoted R^2) of the entire N and K data sets for all samples is ~0.01; however, this coefficient is not very useful for describing small data sets with multiple possible trends, not all of which are necessarily linear. Moreover, the N and K concentrations are affected by the closure of the compositional data set (e.g. Rollinson 1993), further reducing the quantitative value of measures like R^2. Therefore, we conclude that the evidence from this study is consistent with but not diagnostic of a role for $NH_4^+ \leftrightarrow K^+$ substitutions in the incorporation of N into the Hurd localty rocks. Most of the samples with higher N concentrations are illite-bearing hyaloclastites or contain possible ichnofossils. Elevated concentrations of N in magmatic rocks are a good indicator of sedimentary/organic enrichments in the rocks (Li *et al.* 2007; Bebout *et al.* in press). Nitrogen, although a major component of the modern Earth's atmosphere and a key element in biologic evolution (Libourel *et al.* 2003), occurs in very low concentrations in magmatic rocks due to its low solubility and incompatible behaviour, the latter which causes it to degas very efficiently during cooling and crystallization (Marty & Humbert 1997). Typical concentrations of N in fresh, MORB-like basalts, representing residual N trapped in the rocks during the degassing, are between 0.3 and 2.8 ppm with an average around 1.1 ppm (Busigny *et al.* 2005a). Modern hydrothermally altered basalts have elevated N concentrations (Marty 1995; Marty & Humbert 1997; Busigny *et al.* 2005b; Li *et al.* 2007) relative to unaltered equivalents, approaching 20 ppm in rocks that are thought to have experienced high water–rock ratio interactions (see Figs 4(m) and 7; Li *et al.* 2007).

The $\delta^{15}N$ values for the Hurd Property neither co-vary with N contents nor show distinct ranges for any sample type or volcanic unit. The $\delta^{15}N$ of the mantle is inferred to be about −5‰, a value supported by both studies of diamonds and measurements of fresh and lightly altered modern oceanic basalts (Marty & Humbert 1997). The mantle $\delta^{15}N$ value is carried over to fresh basalts, as little to no fractionation occurs during magmatic degassing of N_2 (Marty & Humbert 1997). Hydrothermal alteration

https://doi.org/10.1017/S1473550417000441 Published online by Cambridge University Press

causing N enrichment commonly also increases the basalt whole-rock $\delta^{15}N$. Li *et al.* (2007) reported values approaching +1‰ in hydrothermally altered volcanics in the upper part of the oceanic crust section at ODP Site 801C, attributing the increase to input from seafloor sediments, the latter with values of −0.9 to +5.0‰ in the Marianas margin and +2.5 to +8.2‰ in the Izu margin (data for sediments in Sadofsky & Bebout 2004). Large down-hole $\delta^{15}N$ shifts in the sediment sections are attributed to biologic fractionation of organic N and varying degrees of later diagenetic alteration. The story of the Hurd samples is not well constrained, but all but three of the samples showed positive $\delta^{15}N$ values mostly >+2‰ (Fig. 11). The lowest $\delta^{15}N$ value of −4‰ is still greater than values for MORB and therefore consistent with mixing of mantle and biologically fractionated N. The ichnofossil-bearing samples, which have the greatest N contents of their respective units, generally exhibit $\delta^{15}N$ higher than the values characteristic of chemolithoautotrophic biomass (Fig. 11). Therefore, it seems plausible that the Hurd volcanic rocks were altered by fluids bearing sedimentary/organic N isotope signatures (i.e. that had previously exchanged chemically/isotopically with N in nearby sediments and/or biogeochemically processed N dissolved in seawater). The isotopic signature of these distal and local organic reservoirs is preserved in the Hurd Property volcanic rocks despite significant later metamorphism. Therefore, whereas whole-rock N isotope compositions alone cannot unambiguously identify biologic remains or signatures left behind in the putative trace fossils, they do appear to preserve a record of Archæan biogeochemical N cycling conveyed into the rocks by infiltrating pore waters.

Implications for extraterrestrial habitats

The vastness of the deep subsurface biosphere on Earth, including that residing in basaltic oceanic crust, has only recently been realized, and various studies estimate that anywhere between 6×10^5 and 1×10^9 cells per gram of rock exist in modern seafloor basalts (Einen *et al.* 2008; Santelli *et al.* 2008). Others estimate that approximately two-thirds of Earth's prokaryotic biomass is contained in the deep subseafloor (Whitman *et al.* 1998; Parkes *et al.* 2011). Not all of the organisms present in the subseafloor actively dissolve basaltic glass for redox reaction-derived energy; instead, a great diversity of bacteria (and some Archæa) exist within the various temperature and chemical gradients of the hydrothermal systems in the ocean crust performing both chemoautotrophic and heterotrophic metabolic reactions (Mason *et al.* 2009). The realization of a large biosphere hosted in the deep subsurface, and the expanding range of physicochemical conditions under which microbial life can survive and thrive, have many implications for astrobiology, notably an expansion in a range of plausibly habitable environments. The Martian deep subsurface is thought to be one of the best candidates for an extant Martian biosphere (e.g. Ivarsson & Lindgren 2010). Furthermore, the Martian subsurface may be more suitable for life than Earth's, or provide a greater volume to inhabit, due to the lower heat flow on Mars (Ivarsson & Lindgren 2010). Recent investigations of Martian meteorites (e.g. Cannon *et al.* 2015) and of Martian surface rocks (e.g. Blake *et al.* 2013) show that glass-rich materials are widely distributed on Mars. Our results show that palagonitized basaltic glasses can retain N chemical and isotopic records for ~Ga timescales, underscoring the potential importance of glass alteration processes in recording ancient Martian (bio)geochemical cycles. Incorporation of N into palagonitized volcanic (and impact-related) glasses, in intact volcanic rocks or in soils derived therefrom, could result in appreciable storage of N at/near the Mars surface (cf. Mancinelli & Banin 2003; see Bebout *et al.* 2013). Silicate N within palagonitized glass is distinct from the oxidized N detected at the Martian surface, which is predominantly hosted in highly soluble nitrates (Stern *et al.* 2015). Nitrogen incorporated into palagonitized glass is less susceptible to postformation alteration than nitrates and is therefore a potentially more robust recorder of ancient N. Plausible Martian scenarios for N incorporation into palagonitized basaltic glass include hydrothermal alteration of glass-rich rocks associated with endogenic magmatism and in impact-generated hydrothermal systems, situations that may have been more common in the distant past. Interpretation of such a record will depend on improved constraints on the concentration, isotopic composition and material hosts of N in the Martian surface and interior, from meteorites, *in situ* observations by spacecraft and ultimately from returned samples.

Conclusions

At the ~2.7 Ga outcrop of subaqueous, tholeiitic basaltic andesite volcanics at the Hurd Property, subvertically oriented flows of alternating massive and brecciated glassy flows were sampled at a high resolution for petrographic and geochemical investigation. The units are altered to a maximum grade of greenschist facies, most likely by hydrothermal fluids heated during volcanic activity associated with subsequent seafloor volcanic eruptions reflected in the section preserved at this locality. Petrographic evidence demonstrates that the glasses of the brecciated units experienced early alteration by low-temperature seawater, as indicated by the palagonite phase textures in the hyaloclastite samples. The hyaloclastite flows were more permeable than the holocrystalline massive flows, and therefore experienced the largest amount of element exchange with altering fluids during the water–rock interactions. This is demonstrated by the large variations in the concentrations of relatively fluid-mobile elements, such as K, Rb, Ba, Sr, Li and B, in the hyaloclastite units compared with near uniform concentrations of the same elements in the massive flows. Variations in the concentrations of fluid-mobile elements in the hyaloclastite units are interpreted to reflect the varying surface area to volume ratios of the glass shards, which would affect their permeability and alteration rate. Middle parts of the thicker hyaloclastite flows likely experienced eruption-fed turbidity currents, which would cause high rates of granular collisions resulting in very fractured and rounded glass shards. The top and bottom horizons of the hyaloclastite flows, which contacted either cold seawater or older, cool lava tops, formed as chilled zones where the glass autobrecciated and was essentially 'frozen' into place. It is these flow-top, cuspate glass clasts that appear to have provided the best habitat for euendolithic microorganisms because low glass surface area to volume ratios caused only rims of palagonite to form on the individual shards and preserved glass at the core for microbial colonization. Euendolithic organisms capable of etching glass and leaving behind tubular or granular textures were well established by the Late Archæan. Nitrogen concentration and isotope data presented here show that records of ancient N (bio)geochemical processes can be retained for billions of years in altered basaltic rocks. The silicate N concentrations and $\delta^{15}N$ data from the Hurd Property also suggest that biologically driven processes, specifically denitrification, were active in ocean basins by the time of the Hurd outcrop volcanic eruptions near 2.7 Ga.

https://doi.org/10.1017/S1473550417000441 Published online by Cambridge University Press

Supplementary material. The supplementary material for this article can be found at https://doi.org/10.1017/S1473550417000441

Acknowledgements. This paper largely presents the M.S. thesis research conducted by LDA at the Lehigh University (Anderson 2010). The authors thank Dr Lisa A. Gilbert, from the Williams College-Mystic Seaport Program, for advising and organizing the fieldwork, and the Keck Geology Consortium and the National Science Foundation for funding the field and analytical work. GEB received support from the National Science Foundation, specifically grant EAR-0711355. MRMI acknowledges support from the Mineralogical Association of Canada, and the NSERC CREATE Canadian Astrobiology Training Program. NRB also acknowledges support from NSERC. The authors also thank Editor-in-chief Dr Rocco Mancinelli, and the anonymous reviewer (s) for many insightful comments that led to significant improvements in the manuscript.

References

Alt JC (2003) Hydrothermal fluxes at mid-ocean ridges and on ridge flanks. *Comptes Rendus Geoscience* **335**, 853–864.

Alt JC, Laverne C, Vanko DA, Tartarotti P, Teagle DAH, Bach W, Zuleger E, Erzinger J, Honnorez J, Pezard PA, Becker K, Salisbury MH and Wilkens RH (1996) Hydrothermal alteration of a section of upper oceanic crust in the Eastern Equatorial Pacific: a synthesis of results from site 504 (DSDP Legs 69, 70, and 83, and ODP Legs 111, 137, 140, and 148). In Alt JC, Kinoshita H, Stokking LB and Michael PJ (eds). *Proc. of the Ocean Drilling Program, Scientific Results*, vol. **148**, College Station, TX, USA: Ocean Drilling Program, pp. 417–434.

Anbar AD and Knoll AH (2002) Proterozoic ocean chemistry and evolution: a bioinorganic bridge? *Science* **297**(5584), 1137–1142.

Anderson LD (2010) *Late Archean subaqueous volcanic eruption, hydrothermal alteration, and microbial colonization: evidence from the Abitibi greenstone belt*. Bethlehem, PA, USA: M.S. thesis, Lehigh Univ.

Arndt NT (2004) Crustal growth rates. In Eriksson PG, Altermann W, Nelson DR, Mueller WU, Catuneanu O (eds). *The Precambrian Earth: Tempos and Events. Developments in Precambrian Geology*, vol. **12**. Amsterdam: Elsevier, pp. 155–158.

Ayer J, Ameline Y, Corfu F, Kamo S, Ketchum J, Kwok K and Trowell N (2002) Evolution of the southern Abitibi greenstone belt based on U-Pb geochronology: autochthonous volcanic construction followed by plutonism, regional deformation and sedimentation. *Precambrian Research* **115**, 63–95.

Banerjee NR, Furnes H, Muehlenbachs K, Staudigel H and de Wit M (2006) Preservation of ~3.4–3.5 Ga microbial biomarkers in pillow lavas and hyaloclastites from the Barberton Greenstone Belt, South Africa. *Earth and Planetary Science Letters* **241**, 707–722.

Banerjee NR, Simonetti A, Furnes H, Muehlenbachs K, Staudigel H, Heaman L and Van Kranendonk MJ (2007) Direct dating of Archean microbial ichnofossils. *Geology* **35**(6), 487–490.

Beaumont V and Robert F (1999) Nitrogen isotope ratios of kerogens in Precambrian cherts: a record of the evolution of atmospheric chemistry? *Precambrian Research* **96**, 63–82.

Bebout GE, Idleman BD, Li L and Hilkert A (2007) Isotope-ratio-monitoring gas chromatography methods for high-precision isotopic analysis of nanomole quantities of silicate nitrogen. *Chemical Geology* **240**, 1–10.

Bebout GE, Fogel ML and Cartigny P (2013) Nitrogen: highly volatile yet surprisingly compatible. *Elements* **9**, 333–338.

Bebout GE, Banerjee NR, Izawa MRM, Kobayashi K, Lazzeri K, Ranieri LA and Nakamura E (2017) Nitrogen concentrations and isotopic compositions of seafloor-altered terrestrial basaltic glass: implications for astrobiology. *Astrobiology* **18**(4), 1–13. DOI: 10.1089/ast.2017.1708.

Berger BR & Amelin Y (1999) Geological investigations in Guibord, Michaud and Garrison Townships. In *Summary of Field Work and Other Activities*. Ontario Geological Survey Miscellaneous Paper. Sudbury, ON, Canada: Ontario Geological Survey, pp. 25–32.

Blake DF, Morris RV, Kocurek G, Morrison SM, Downs RT, Bish D, Ming DW, Edgett KS, Rubin D, Goetz W, Madsen MB, Sullivan R, Gellert R, Campbell I, Treiman AH, McLennan SM, Yen AS, Grotzinger J, Vaniman DT, Chipera SJ, Achilles CN, Rampe EB, Sumner D, Meslin PY, Maurice S, Forni O, Gasnault O, Fisk M, Schmidt M, Mahaffy P, Leshin LA, Glavin D, Steele A, Freissinet C, Navarro-Gonzalez R, Yingst RA, Kah LC, Bridges N, Lewis KW, Bristow TF, Farmer JD, Crisp JA, Stolper EM, Des Marais DJ and Sarrazin P (2013) Curiosity at Gale Crater, Mars: characterization and analysis of the Rocknest sand shadow. *Science* **341**, 1–8. DOI: 10.1126/science.1239505.

Borthwick J and Harmon RS (1982) A note regarding ClF_3 as an alternative to BrF_5 for oxygen isotope analysis. *Geochimica et Cosmochimica Acta* **46**, 1665–1668.

Bowers TS (1989) Stable isotope signatures of water-rock interaction in mid-ocean ridge hydrothermal systems: sulfur, oxygen, and hydrogen. *Journal of Geophysical Research* **94**(B5), 5775–5786.

Boyd SR (2001) Nitrogen in future biosphere studies. *Chemical Geology* **176**, 1–30.

Bridge NJ (2008) *Traces of early life from volcanic rocks of the Abitibi greenstone belt*. London, ON, Canada: Honors Undergraduate Thesis, University of Western Ontario, 155p.

Bridge NJ, Banerjee NR, Mueller W, Muehlenbachs K and Chacko T (2010) A volcanic habitat for early life preserved in the Abitibi Greenstone belt Canada. *Precambrian Research* **179**(1–4), 88–98. doi: 10.1016/j.precamres.2010.02.017.

Brocks JJ, and Logan GA, Buick R and Summons RE (1999) Archean molecular fossils and the early rise of eukaryotes. *Science* **285**, 1033–1036.

Busigny V, Ader M and Cartigny P (2005a) Quantification and isotopic analysis of nitrogen in rocks at the ppm level using sealed tube combustion technique: a prelude to the study of altered oceanic crust. *Chemical Geology* **223**, 249–258.

Busigny V, Laverne C and Bonifacie M (2005b) Nitrogen content and isotopic composition of oceanic crust at a superfast spreading ridge: a profile in altered basalts from ODP site 1256, Leg 206. *Geochemistry, Geophysics, Geosystems* **6**(12), 1–16. doi: 10.1029/2005GC001020.

Cannon KM, Mustard JF and Agee CB (2015) Evidence for a widespread basaltic breccia component in the Martian low-albedo regions from the reflectance spectrum of Northwest Africa 7034. *Icarus* **252**(15), 150–153.

Card KD (1990) A review of the Superior Province of the Canadian Shield, a product of Archean accretion. *Precambrian Research* **48**, 99–156.

Chan L-H, Alt JC and Teagle DAH (2002) Lithium and lithium isotope profiles through the upper oceanic crust: a study of seawater-basalt exchange at ODP sites 504B and 896A. *Earth and Planetary Science Letters* **201**, 187–201.

Clayton RN and Mayeda TK (1963) The use of bromine-pentafluoride in the extraction of oxygen from oxides and silicates for isotopic analysis. *Geochimica et Cosmochimica Acta* **27**, 43–52.

Condie KC (1981) Archean greenstone belts. In Condie KC (ed.). *Developments in Precambrian Geology 3*. Amsterdam: Elsevier Scientific Publishing Company, pp. 433.

Davies GF (1980) Thermal histories of convective Earth models and constraints on radiogenic heat production in the Earth. *Journal of Geophysical Research* **85**(B5), 2517–2530.

Dimroth E, Imreh L, Rocheleau M and Goulet N (1982) Evolution of the south-central part of the Archean Abitibi Belt, Quebec, Part I: stratigraphy and paleogeographic model. *Canadian Journal of Earth Sciences* **19**, 1729–1758.

Dimroth E, Imreh L, Goulet N and Rocheleau M (1983a) Evolution of the south-central segment of the Archean Abitibi Belt Quebec Part II: tectonic evolution and geomechanical model. *Canadian Journal of Earth Sciences* **20**, 1355–1373.

Dimroth E, Imreh L, Goulet N and Rocheleau M (1983b) Evolution of the south-central segment of the Archean Abitibi Belt Quebec Part III: plutonic and metamorphic evolution and geotectonic model. *Canadian Journal of Earth Sciences* **20**, 1374–1388.

Einen J, Thorseth IH and Øvreås L (2008) Enumeration of *Archaea* and *Bacteria* in seafloor basalt using real-time quantitative PCR and fluorescence microscopy. *FEMS Microbiology Letters* **282**, 182–187.

Falkowski PG and Godfrey LV (2008) Electrons, life and the evolution of Earth's oxygen cycle. *Philosophical Transactions of the Royal Society of London* **B363**, 2705–2716.

Fisk MR, Giovannoni SJ and Thorseth IH (1998) Alteration of oceanic volcanic glass: textural evidence of microbial activity. *Science* **281**, 978–980.

Fogel ML (2010) Variations of abundances of nitrogen isotopes in nature. In Beauchemin D, Matthews DE (eds) *The Encyclopedia of Mass Spectrometry*, vol. **5**. Amsterdam: Elsevier, pp. 842–852.

Furnes H, Thorseth IH, Tumyr O, Torsvik T and Fisk MR (1996) Microbial activity in the alteration of glass from pillow lavas from Hole 896A. In Alt JC, Kinoshita H, Stokking LB and Michael PJ (eds). *Proc. of the Ocean Drilling Program, Scientific Results*, vol. **148**. College Station, TX, USA: Ocean Drilling Program, pp. 191–206.

Furnes H, Banerjee NR, Muehlenbachs K, Staudigel H and de Wit M (2004) Early life recorded in Archean pillow lavas. *Science* **34**, 578–581.

Furnes H, Banerjee NR, Staudigel H, Muehlenbachs K, McLoughlin N, de Wit M and Van Kranendonk M (2007) Comparing petrographic signatures of bioalteration in recent to Mesoarchean pillow lavas: tracing subsurface life in oceanic igneous rocks. *Precambrian Research* **158**, 156–176.

Garvin J, Buick R, Anbar AD, Arnold GL and Kaufman AJ (2009) Isotopic evidence for an aerobic nitrogen cycle in the latest Archean. *Science* **323**, 1045–1048.

Godfrey LV and Falkowski PG (2009) The cycling and redox state of nitrogen in the Archaean ocean. *Nature Geoscience* **2**, 725–729.

Godfrey LV, Poulton SW, Bebout GE and Fralick P (2013) Stability of the nitrogen cycle during development of sulfidic water in the redox-stratified late Paleoproterozoic Ocean. *Geology* **41**(6), 655–658. doi: 10.1130/G33930.1.

Gregory RT and Taylor HP Jr (1981) An oxygen isotopic profile in a section of Cretaceous oceanic crust, Samail Ophiolite, Oman: evidence for $\delta^{18}O$ buffering of the oceans by deep (>5 km) seawater-hydrothermal circulation at mid-ocean ridges. *Journal of Geophysical Research* **86**(B4), 2737–2755.

Gutzmer J, Banks DA, Lüders V, Hoefs J, Beukes NJ and von Bezing KL (2003) Ancient sub-seafloor alteration of basaltic andesites of the Ongeluk Formation, South Africa: implications for the chemistry of Paleoproterozoic seawater. *Chemical Geology* **201**, 37–53.

Hannington MD, Santaguida F, Kjarsgaard IM and Cathles LM (2003) Regional-scale hydrothermal alteration in the Central Blake River Group, western Abitibi subprovince, Canada: implications for VMS prospectivity. *Mineralium Deposita* **38**, 393–422.

Hashizume K, Sugihara A, Pinti DL, Orberger B and Westall F (2006) Search for primordial biogenic isotopic signatures of nitrogen in Archean sedimentary rocks. *Geochimica et Cosmochimica Acta* **70**(Suppl. 1), A235.

Hofmann A and Harris C (2008) Silica alteration zones in the Barberton greenstone belt: a window into subseafloor processes 3.5–3.3 Ga ago. *Chemical Geology* **257**, 224–242.

Holden JR and Dickinson CW (1975) Crystal structures of three solid solution phases of ammonium nitrate and potassium nitrate. *Journal of Physical Chemistry* **79**(3), 249–256.

Holland HD (2006) The oxygenation of the atmosphere and oceans. *Philosophical Transactions of the Royal Society B: Biological Sciences* **361** (1470), 903–915.

Hollocher K, Robinson P, Walsh E and Roberts D (2012) Geochemistry of amphibolite-facies volcanics and gabbros of the Støren Nappe in extensions west and southwest of Trondheim, Western Gneiss Region, Norway: a key to correlations and paleotectonic settings. *The American Journal of Science* **312**, 357–416.

Ivarsson M and Lindgren P (2010) The search for sustainable subsurface habitats on Mars, and the sampling of impact ejecta. *Sustainability* **2**, 1969–1990.

Izawa MRM, Banerjee NR, Flemming RL, Bridge NJ and Schultz C (2010) Basaltic glass as a habitat for microbial life: implications for astrobiology and planetary exploration. *Planetary and Space Science* **58**(4), 583–591. doi: 10.1016/j.pss.2009.09.014.

Jackson SL, Fyon JA and Corfu F (1994) Review of Archean supracrustal assemblages of the southern Abitibi greenstone belt in Ontario, Canada: products of microplate interaction within a large-scale plate-tectonic setting. *Precambrian Research* **65**, 183–205.

Jia Y and Kerrich R (2004) Nitrogen 15-enriched Precambrian kerogen and hydrothermal systems. *Geochemistry, Geophysics, Geosystems* **5**(7), 1–21. doi: 10.1029/2004GC000716.

Jones MI (1992) *Variolitic basalts: relations to Archean epigenetic gold deposits in the Abitibi Greenstone belt*. Unpub. Ottawa, ON, Canada: MS Thesis, University of Ottawa, 320p.

Kashefi K and Lovley DR (2003) Extending the upper temperature limit for life. *Science* **301**, 934.

Kruber C, Thorseth IH and Pedersen RB (2008) Seafloor alteration of basaltic glass: textures, geochemistry and endolithic microorganisms. *Geochemistry, Geophysics, Geosystems* **9**, Q12002. doi: 10.1029/2008GC002119.

Kump LR (2008) The rise of atmospheric oxygen. *Nature* **451**, 277–278.

LeBas MJ, LeMaitre RW, Streckeisen A and Zanettin B (1986) A chemical classification of volcanic rocks based on the total alkali-silica diagram. *Journal of Petroleum* **27**, 745–750.

Li L, Bebout GE and Idleman BD (2007) Nitrogen concentration and $\delta^{15}N$ of altered oceanic crust obtained on ODP Legs 129 and 185: insights into alteration-related nitrogen enrichment and the nitrogen subduction budget. *Geochimica et Cosmochimica Acta* **71**, 2344–2360.

Libourel G, Marty B and Humbert F (2003) Nitrogen solubility in basaltic melt. Part I. Effect of oxygen fugacity. *Geochimica et Cosmochimica Acta* **67**(21), 4123–4135.

Lowell RP, Rona PA and Von Herzen RP (1995) Seafloor hydrothermal systems. *Journal of Geophysical Research* **100**, 327–352.

Mancinelli RL and Banin A (2003) Where is the nitrogen on Mars? *International Journal of Astrobiology* **2**, 217–225.

Marty B (1995) Nitrogen content of the mantle inferred from N_2-Ar correlation in oceanic basalts. *Nature* **377**, 326–329.

Marty B and Humbert F (1997) Nitrogen and argon isotopes in oceanic basalts. *Earth and Planetary Science Letters* **152**, 101–112.

Mason OU, Di Meo-Savoie CA, Van Nostrand JD, Zhou J, Fisk MR and Giovannoni SJ (2009) Prokaryotic diversity, distribution, and insights into their role in biogeochemical cycling in marine basalts. *International Society for Microbial Ecology Journal* **3**, 231–242.

McDonough WF and Sun SS (1995) The Composition of the Earth. *Chemical Geology* **120**, 223–253.

McLoughlin N, Staudigel H, Furnes H, Eickmann B and Ivarsson M (2010) Mechanisms of microtunneling in rock substrates – distinguishing endolithic biosignatures from abiotic microtunnels. *Geobiology* **8**, 245–255.

Muehlenbachs K (1986) Alteration of the oceanic crust and the ^{18}O history of seawater. In Valley JW, Taylor HP Jr & O'Neil JR (eds). *Stable Isotopes in High Temperature Geological Processes Rev Mineral*, vol. **16**. Chantilly, VA, USA: Mineralogical Society of America, pp. 425–444.

Muehlenbachs K and Clayton RN (1972) Oxygen isotope studies of fresh and weathered submarine basalts. *The Canadian Journal of Earth Sciences* **9**(2), 172–184.

Mueller W and Daigneault R (2006) Evolution of the Abitibi greenstone belt. In Mueller WU, Daigneault R, Pearson V, Houle M, Dostal J, Pilote P (eds). *The Komatiite-komatiitic Basalt-basalt Association in Oceanic Plateaus and Calderas: Physical Volcanology and Textures of Subaqueous Archean Flow Fields in the Abitibi Greenstone Belt, GAC-MAC Excursion A3, Montreal*. Montreal, QC, Canada: Geological Association of Canada/Mineralogical Association of Canada, pp. 4–10.

Mueller WU, Daigneault R, Mortensen JK and Chown EH (1996) Archean terrane docking: upper crust collision tectonics, Abitibi greenstone belt, Quebec, Canada *Tectonophysics* **265**, 127–150.

Parkes RJ, Linnane CD, Webster G, Sass H, Weightman AJ, Hornibrook ERC and Horsfield B (2011) Prokaryotes stimulate mineral H_2 formation for the deep biosphere and subsequent thermogenic activity. *Geology* **39**, 219–222.

Pearson V and Daigneault R (2009) An Archean megacaldera complex: the Blake River Group, Abitibi Greenstone Belt. *Precambrian Research* **168**, 66–82.

Pinti DL, Hashizume K, Orberger B, Gallien J-P, Cloquet C and Massault M (2007) Biogenic nitrogen and carbon in Fe-Mn-oxyhydroxides from an Archean chert, Marble Bar, Western Australia. *Geochemistry, Geophysics, Geosystems* **8**(2), 1–19. doi: 10.1029/2006GC001394.

Rollinson H (1993) *Using Geochemical Data; Evaluation, Presentation Interpretation* Harlow, UK: Longman Scientific and Technical, 352 pp.

Rosing MT (1999) ^{13}C-Depleted carbon microparticles in >3700-Ma sea-floor sedimentary rocks from West Greenland. *Science* **283**, 674–676.

Sadofsky SJ and Bebout GE (2004) Nitrogen geochemistry of subducting sediments: new results from the Izu-Bonin-Mariana margin and insights regarding global nitrogen subduction. *Geochemistry, Geophysics, Geosystems* **5**, Q03I15. doi: 10.1029/2003GC000543.

Santelli CM, Orcutt BN, Banning E, Bach W, Moyer CL, Sogin ML, Staudigel H and Edwards KJ (2008) Abundance and diversity of microbial life in ocean crust. *Nature* **453**, 653–657.

Schopf JW (2004) Earth's earliest biosphere: status of the hunt. In Eriksson PG, Altermann W, Nelson DR, Mueller WU, Catuneanu O (eds). *The Precambrian Earth: Tempos and Events Develop Precambr. Geol.*, vol. **12**. Amsterdam: Elsevier, pp. 516–539.

Scott C, Richard D and Fowler AD (2003) An Archean submarine pyroclastic flow: the Hurd Deposit, Harker Township, Ontario Canada *American Geophysical Union Special Volume on Explosive Volcanism, Geophysical Monograph* **140**, 317–327.

Shannon RD (1976) Revised effective ionic radii and systematic studies of interatomic distances in halides and chalcogenides. *Acta Crystallographica Section A* **32**(5), 751–767.

Staudigel H, Plank T, White B, Schmincke HU (1996) Geochemical fluxes during seafloor alteration of the basaltic upper oceanic crust: DSDP sites 417 and 418. In Bebout GE, Scholl DW, Kirby SH, Platt JP (eds). *Subduction: Top to Bottom*. Washington, DC: American Geophysical Union, pp. 19–38.

Staudigel H, Furnes H, Banerjee NR, Dilek Y and Muehlenbachs K (2006) Microbes and volcanoes: a tale from the oceans, ophiolites, and greenstone belts. *GSA Today* **16**(10), 4–10.

Staudigel H, Furnes H, McLoughlin N, Banerjee NR, Connell LB and Templeton A (2008) 3.5 billion years of glass bioalteration: volcanic rocks as a basis for microbial life? *Earth-Science Reviews* **89**, 156–176.

Stern JC, Sutter B, Freissinet C, Navarro-Gonzalez R, McKay CP, Archer PD Jr, Buch A, Brunner AE, Coll P, Eigenbrode JL, Fairen AG, Franz HB, Glavin DP, Kashyap S, McAdam AC, Ming DW, Steele A, Szopa C, Wray JJ, Martin-Torres FJ, Zorzano M-P, Conrad PG, Mahaffy PR and The MSL Science Team (2015) Evidence for indigenous nitrogen in sedimentary and Aeolian deposits from the curiosity rover investigations at Gale crater Mars *Proceedings of the National Academy of Science of the USA* **112**, 4245–4250. doi: 10.1073/pnas.1420932112.

Stroncik NA and Schmincke H-U (2001) Evolution of palagonite: crystallization, chemical changes, and elemental budget. *Geochemistry, Geophysics, Geosystems* **2**, 2000GC000102.

Stroncik NA and Schmincke H-U (2002) Palagonite – a review. *The International Journal of Earth Sciences* **91**, 680–697.

Thomazo C and Papineau D (2013) Biogeochemical cycling of nitrogen on the early Earth. *Elements* **9**(5), 345–352.

Thomazo C, Ader M and Philippot P (2010) Extreme ^{15}N-enrichments in 2.72-Gyr-old sediments: evidence for a turning point in the nitrogen cycle. *Geobiology* **9**, 107–120.

White JDL (2004) Explosive subaqueous volcanism. In Eriksson PG, Altermann W, Nelson DR, Mueller WU, Catuneanu O (eds). *The Precambrian Earth: Tempos and Events Developments in Precambrian Geology*, vol. **12**. Amsterdam: Elsevier, pp. 334–345.

Whitman WB, Coleman DC and Wiebe WJ (1998) Prokaryotes: the unseen majority. *Proceedings of the National Academy of Sciences of the USA* **95** (12), 6578–6583.

Winchester JA and Floyd PA (1977) Geochemical discrimination of different magma series and their differentiation products using immobile elements. *Chemical Geology* **20**, 325–343.

Zerkle AL and Mikhail S (2017) The geobiological nitrogen cycle: from microbes to the mantle. *Geobiology* **15**(3), 343–352. doi: 10.1111/gbi.12228.

Zhou ZH, Fyfe WS, Tazaki K and Vandergaast SJ (1992) The structural characteristics of palagonite from DSDP site-335. *Candian Mineralogist* **30**, 75–81.